

Quantum Dragon Solutions for Electron Transport through Nanostructures based on Rectangular Graphs

G. Inkoom and M.A. Novotny*
Department of Physics and Astronomy
Mississippi State University
Mississippi State, MS 39762-5167 USA
 (Dated: September 19, 2018)

Electron transport through nanodevices of atoms in a single-layer rectangular arrangement with free (open) boundary conditions parallel to the direction of the current flow is studied within the single-band tight binding model. The Landauer formula gives the electrical conductance to be a function of the electron transmission probability, $\mathcal{T}(E)$, as a function of the energy E of the incoming electron. A quantum dragon nanodevice is one which has a perfectly conducting channel, namely $\mathcal{T}(E) = 1$ for all energies which are transmitted by the external leads even though there may be arbitrarily strong electron scattering. The rectangular single-layer systems are shown to be able to be quantum dragon devices, both for uniform leads and for dimerized leads. The quantum dragon condition requires appropriate lead-device connections and correlated randomness in the device.

PACS numbers: 73.63.-b, 78.67.Bf, 85.35.-p

Keywords: Electron Transport, Quantum Dragons, Nanodevices

I. INTRODUCTION

The confluence of the approaching end of Moore's law for electronics¹ and the increasing ability of experimentally being able to manipulate, fabricate, and measure at the nanoscale level² is the reason rapid progress in nano-electronics is being made³. Of particular interest is the electron transmission properties of nanodevices⁴⁻⁷, including electron transmission in molecular electronics^{8,9}.

Due to the quantum mechanics underlying nanodevices, properties of coherent electron transport can be very different from those expected at the macroscopic scale. As shown by Landauer¹⁰, of central importance to nanodevices is the electron transmission, \mathcal{T} , of the nanodevice when it is connected to leads attached to a source and a sink of electrons. As in macroscopic systems, one desires the electrical conductance G (the inverse of the electrical resistance) in an Ohm's law relationship $I = GV$ where I is the electrical current flowing through the device and V is the applied electrical voltage difference. At low temperatures the Landauer formula gives the electrical conductance^{5,11}

$$G = \begin{cases} G_0 \mathcal{T}(E_F) & \text{two probe} \\ G_0 \frac{\mathcal{T}(E_F)}{1-\mathcal{T}(E_F)} & \text{four probe} \end{cases} \quad (1)$$

for two probe or four probe measurements. Here $G_0 = \frac{2e^2}{h}$ is the quantum of conductance, with e the charge of the electron, h Planck's constant, and the factor of two is due to the spin of the electron. The transmission is a function of the energy E of an incoming electron, and in Eq. (1) the transmission at the Fermi energy E_F enters. The power of the shot noise of the nanodevice is¹²⁻¹⁵

$$P = \frac{4e^3}{h} \mathcal{T}(E_F) [1 - \mathcal{T}(E_F)] V \quad (2)$$

which is zero if $\mathcal{T}(E_F)=1$.

In this investigation we are interested in a perfectly conducting channel, namely where $\mathcal{T}(E) = 1$ for all energies E which can propagate through long leads. There are different possibilities for the existence of perfectly conducting channels in coherent electron propagation. These possibilities include:

- **Ballistic propagation.**

If there is no scattering in the device, electrons propagate ballistically, and $\mathcal{T}(E) = 1$. For ballistic propagation, the two different behaviors for G in Eq. (1) have been observed experimentally in the same sample of a very pure semiconductor¹⁶.

- **Long-range randomness.**

For example, in zigzag carbon nanoribbons when there is random long-range scattering, the average $\langle G \rangle \rightarrow G_0$ in two probe measurements as the length L of the device increases¹⁷.

- **Surface states in topological insulators.**

In topological insulators, surface states can lead to perfectly conducting channels which are protected against scattering due to disorder¹⁸.

- **Quantum dragons.**

In 2014, one of the authors discovered a large class of nanodevices¹⁹ which can have arbitrarily strong scattering, but because the scattering is correlated they can have $\mathcal{T}(E)=1$ for any L . These nanodevices, with strong scattering but with a perfectly conducting channel, were named 'quantum dragons' in ref. 19.

Sometimes nanodevices with a perfectly conducting channel have been said to be metallic or ballistic, due to the electrical conductance given by Eq. (1). Examples are armchair single walled carbon nanotubes^{20,21} and graphene nanoribbons^{22,23}. TEM and SEM investigations of gold point contacts have also been performed²⁵.

Single layer thick carbon nanotubes and graphene nanoribbons have been fabricated, and their intriguing properties studied^{22,23}. These systems are all based on an underlying hexagonal lattice. Single-walled carbon nanotubes in the armchair arrangement have been experimentally shown to have metallic behavior²⁰, often in the literature said to exhibit ballistic electron propagation²⁴. However, one needs to be careful to remember $\mathcal{T}(E) = 1$ only if an armchair single-walled carbon nanotube is connected to appropriate leads in the correct fashion^{19,20}.

The name quantum dragons denotes such devices may be formed by joining different types of nanodevices, their length is typically longer than any other dimension, and they are invisible to electrons which propagate in the leads. The quantum dragon nanodevices published in ref. 19 all had cylindrical symmetry. In this paper we investigate quantum dragon nanodevices without cylindrical symmetry. In particular, we investigate quantum dragons in single-layer thick nanodevices based on an underlying rectangular graph, with open (free) boundary conditions perpendicular to the direction of the current flow.

Recently, some single layer thick materials based on rectangular lattices have been synthesized. One example is free-standing single-atom-thick iron membranes²⁷, and another is copper oxide monolayers^{28,29}. Other examples are 2D materials and van der Waal heterostructures have recently been reviewed³⁰. These experimental systems, and the possibility of many more 2D systems based on rectangular lattices, provide the impetus to study whether nanodevices based on underlying rectangular graphs can have $\mathcal{T}(E)=1$, and in particular whether such systems can be quantum dragons.

The paper is organized as follows. In Sec. II, the method of calculating $\mathcal{T}(E)$ for non-dimerized devices and leads is presented. The method used is the matrix method²⁶. Sec. III gives the method to obtain quantum dragon solutions via the exact mapping and tuning process for systems based on rectangular graphs. Sec. IV contains example numerical calculations of non-dimerized quantum dragons, thereby better illustrating the concept. Sec. V has our conclusions and further discussion. The main text is supplemented with a number of appendices. A detailed discussion of the example devices shown is presented in App. A for devices without disorder and in App. B for devices with disorder. The matrix method to calculate $\mathcal{T}(E)$ for dimerized leads is derived in App. C. Quantum dragon solutions for nanodevices based on rectangular graphs with dimerized leads is presented in App. D. The relationship between the matrix method used in this article and the commonly used Green's function method to calculate $\mathcal{T}(E)$ is given in

App. E. Appendix F shows in mathematical detail how quantum dragon solutions arise in the case of two slices in the nanodevice.

II. TRANSMISSION $\mathcal{T}(E)$ CALCULATIONS

The electron transmission is found from the solution of the time-independent Schrödinger equation for the nanodevice and leads. Although solutions using density functional theory, as in the review⁸, are possible, this imposes a limit on the number of atoms which can be studied in the nanodevice and furthermore limits one to numerical investigations. Therefore, here we study the nanodevice and leads within the single-band tight binding (TB) model. In the TB model the important quantities are the on site energy (at the location of every atom), ϵ , and the hopping between atoms, denoted in this article by either t or s . The hopping terms come from overlaps of electron wavefunctions between atoms located near one another, so in the device and the leads we limit ourselves to nearest-neighbor (nn) and next-nearest-neighbor (nnn) hopping terms. In most cases the hopping terms are negative, so we put in the negative sign 'by hand' and let t or s stand for the magnitude of the hopping. Four advantages of the TB model for electron transport calculations are detailed in ref. 6. We only analyze the two terminal measurement setup. Within the TB model, the matrix equation to solve is

$$(\mathcal{H} - E\mathbf{I}_\infty)\vec{\Psi} = \vec{0} \quad (3)$$

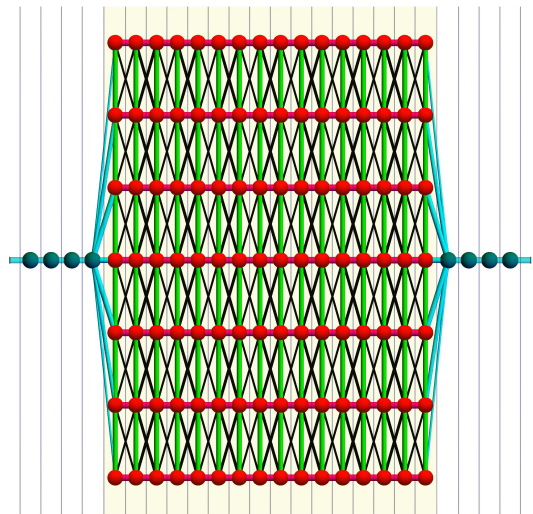


FIG. 1. (Color online.) An example of leads connected to a planar rectangular nanodevice with $\ell = 16$ and $m = 7$. Leads and device are both uniform and without disorder. See Appendix A.1 for a complete description.

where \mathbf{I}_∞ is the infinite identity matrix, \mathcal{H} is the infinite matrix for the two semi-infinite leads and the device, and E is the energy of the incoming electrons.

In the text in the main article, we concentrate on uniform (not dimerized) leads attached to a rectangular device, as in Fig. 1. The case where the leads are dimerized has the matrix method solution derived in App. C and analyzed in App. D. We have freedom in choosing our zero of energy, so we choose the on site energy of the lead atoms to be zero. The hopping strength between lead atoms we take to be t_{lead} . In many cases theorists take t_{lead} to be the unit of energy and set it to unity^{19,26,31,32}, but we will keep t_{lead} throughout in order to make better connection with the dimerized leads in the appendices. We assume our nanodevice has an underlying rectangular graph, as in Fig. 1. Every slice (every column) of the nanodevice has m atoms, and there are ℓ slices. Within column j , every atom has the same on site energy ϵ_j and the same nn hopping t_j . Between columns j and $j+1$ there can be nn hopping of strength $s_{nn,j}$ and nnn hopping of strength $s_{nnn,j}$. The device can be considered to be a planar rectangular array of atoms when there is no

disorder, as in Fig. 1, when all TB parameters are the same, that is $\epsilon_j=\epsilon$, $t_j=t$, $s_{nn,j}=s_{nn}$, and $s_{nnn,j}=s_{nnn}$.

When there is disorder in the TB parameters ϵ_j , t_j , $s_{nn,j}$ and $s_{nnn,j}$, the underlying graph is still rectangular but the nanodevice need not remain planar, as in Fig. 2.

We use the matrix method²⁶ to calculate the transmission, $\mathcal{T}(E)$, because the mapping and tuning method to find quantum dragons takes advantage of the matrix structure. App. E gives the relationship between the commonly used Green's function method^{4-9,33} and the matrix method. For dimerized leads the method is derived in App. C, while for uniform leads the matrix method was put forward in 2000²⁶.

Unless otherwise explicitly stated or indicated by subscripts, the dimension of all vectors is m and all matrices are of size $m \times m$. The transmission is calculated by $\mathcal{T}=|t_T|^2$ where t_T is calculated by the inverse of a $(\ell m+2) \times (\ell m+2)$ matrix \mathbf{M}_ℓ which has the form (written for $\ell=4$)

$$\mathbf{M}_4 \begin{pmatrix} 1+r \\ \vec{\psi}_1 \\ \vec{\psi}_2 \\ \vec{\psi}_3 \\ \vec{\psi}_4 \\ t_T \end{pmatrix} = \begin{pmatrix} \xi & \vec{w}^\dagger & \vec{0}^\dagger & \vec{0}^\dagger & \vec{0}^\dagger & 0 \\ \vec{w} & \mathbf{F}_1 & \mathbf{B}_{12} & \mathbf{0} & \mathbf{0} & \vec{0} \\ \vec{0} & \mathbf{B}_{12}^\dagger & \mathbf{F}_2 & \mathbf{B}_{23} & \mathbf{0} & \vec{0} \\ \vec{0} & \mathbf{0} & \mathbf{B}_{23}^\dagger & \mathbf{F}_3 & \mathbf{B}_{34} & \vec{0} \\ \vec{0} & \mathbf{0} & \mathbf{0} & \mathbf{B}_{34}^\dagger & \mathbf{F}_4 & \vec{u} \\ 0 & \vec{0}^\dagger & \vec{0}^\dagger & \vec{0}^\dagger & \vec{u}^\dagger & \xi \end{pmatrix} \begin{pmatrix} 1+r \\ \vec{\psi}_1 \\ \vec{\psi}_2 \\ \vec{\psi}_3 \\ \vec{\psi}_4 \\ t_T \end{pmatrix} = \begin{pmatrix} \Lambda \\ \vec{0} \\ \vec{0} \\ \vec{0} \\ \vec{0} \\ 0 \end{pmatrix} \quad (4)$$

where the vector \vec{w} (\vec{u}) contains the TB hopping terms between the incoming left (outgoing right) lead and the atoms in the first (last) slice of the device. The intra-slice TB terms, here ϵ_j and t_j , are in the matrices $\mathbf{F}_j = \mathbf{A}_j - E\mathbf{I}$ with \mathbf{I} the $m \times m$ identity matrix. Note the energy E is only present in the diagonal elements of \mathbf{M}_ℓ . The TB intra-slice matrix is

$$\mathbf{A}_j = \epsilon_j \mathbf{I} - t_j \mathbf{Q} \quad \text{for } j = 1, 2, \dots, \ell \quad (5)$$

and the inter-slice TB terms are

$$\mathbf{B}_{j,j+1} = -s_{nn,j} \mathbf{I} - s_{nnn,j} \mathbf{Q}. \quad (6)$$

The matrix \mathbf{Q} is defined by

$$\mathbf{Q} = \begin{pmatrix} 0 & 1 & 0 & \dots & 0 & 0 & 0 \\ 1 & 0 & 1 & & 0 & 0 & 0 \\ 0 & 1 & 0 & \dots & 0 & 0 & 0 \\ \vdots & \vdots & \ddots & \vdots & \vdots & & \\ 0 & 0 & 0 & \dots & 0 & 1 & 0 \\ 0 & 0 & 0 & & 1 & 0 & 1 \\ 0 & 0 & 0 & \dots & 0 & 1 & 0 \end{pmatrix} \quad (7)$$

and has this form because we study a rectangular lattice, allow only nn hopping within each slice, and allow

only nn and nnn hopping between slices. The matrix \mathbf{A}_j contains the part of the Hamiltonian which includes all TB parameters within slice j , while $\mathbf{B}_{j,j+1}$ is the part of the Hamiltonian containing the TB parameters which are the hopping terms between atoms in slices numbered j and $j+1$. The wavevector q of the electron in the leads is given by

$$\cos(q) = -\frac{E}{2t_{lead}} \quad (8)$$

where the distance has been taken to be unity between lead atoms. Hence $\sin(q) = \pm \sqrt{4t_{lead}^2 - E^2}/2t_{lead}$. Furthermore, in Eq. (4) $\Lambda = -2i \sin(q)$ and $\xi = e^{-iq}$. For propagating modes we require $-1 \leq \cos(q) \leq 1$, which give propagating modes for energies $-2t_{lead} \leq E \leq 2t_{lead}$.

III. QUANTUM DRAGON SOLUTIONS VIA EXACT MAPPING

In ref. 19, an exact mapping between a nanodevice with ℓm atoms and a 1D (one dimensional) nanodevice with

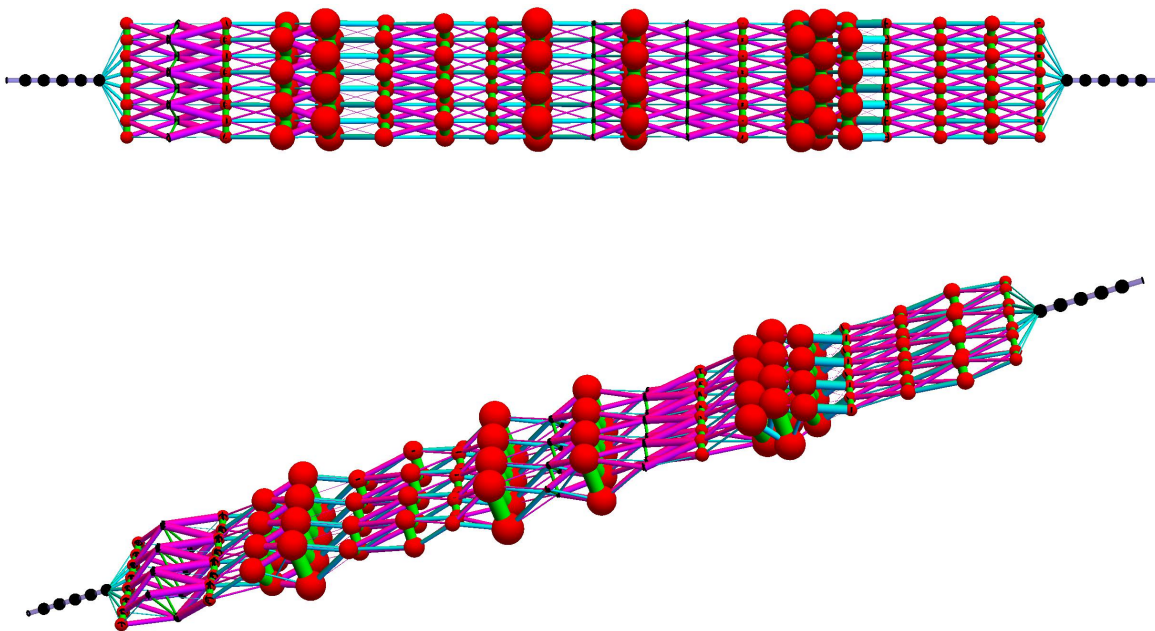


FIG. 2. (Color online.) An example of uniform leads connected to a disordered, rectangular device with $m=8$ and $\ell=20$. The same device is shown in the top (top view) and bottom (oblique view) of the figure. See Appendix B for a complete description.

ℓ atoms was shown to be sometimes possible. The mapping preserves $\mathcal{T}(E)$, and provides a method to find the 1D chain of length ℓ which has the same $\mathcal{T}(E)$ as the nanodevice with ℓm atoms. For some TB parameters in the original nanodevice, the 1D chain mapped onto is identical to a segment of length ℓ of the leads. Consequently, for nanodevices with these parameters, one has $\mathcal{T}(E)=1$ since the 1D mapped system is indistinguishable from a segment of the same length of the leads. For uniform leads, as we study in the main article,¹⁹ gives the requirements for the exact mapping, as well as conditions for a quantum dragon. The matrix method for the solution of $\mathcal{T}(E)$ and the mapping and tuning for dimerized leads and a dimerized device is given in App. C and App. D.

The important consideration for the existence of an exact mapping when all slices have m atoms is that there exists a vector \vec{x}_1 which is simultaneously an eigenvector of all \mathbf{A}_j and all $\mathbf{B}_{j,j+1}$. Note the \mathbf{A}_j are Hermitian, while the $\mathbf{B}_{j,j+1}$ do not need to be Hermitian. Furthermore, the nanodevice must be connected to the uniform leads such that $\vec{w} \propto \vec{x}_1$ and $\vec{u} \propto \vec{x}_1$. Of course for physical nanodevices, \vec{x}_1 must be composed of valid TB hopping parameters. In our case, the \mathbf{A}_j and $\mathbf{B}_{j,j+1}$ are tridiagonal Toeplitz matrices. We restrict ourselves to the case of zero magnetic field, so all TB hopping terms are real. We also restrict nnn hopping between atoms in slice j and $j+1$ to all be identical, so in our case the $\mathbf{B}_{j,j+1}$ matrices are also Hermitian. All our matrices have the form

$$\mathbf{C} = c_I \mathbf{I} + c_Q \mathbf{Q} \quad (9)$$

for some parameters c_I and c_Q , and the matrix \mathbf{Q} is given

in Eq. (7). The matrix in Eq. (9) has eigenvalues³⁴

$$\hat{\lambda}_k = c_I + 2c_Q \cos\left(\frac{k\pi}{m+1}\right) \quad \text{for } k = 1, 2, \dots, m \quad (10)$$

and the eigenvector associated with $\hat{\lambda}_1$ is

$$\vec{x}_1 = \sqrt{\frac{2}{m+1}} \begin{pmatrix} \sin\left(\frac{\pi}{m+1}\right) \\ \sin\left(\frac{2\pi}{m+1}\right) \\ \vdots \\ \sin\left(\frac{m\pi}{m+1}\right) \end{pmatrix} \quad (11)$$

where we note that \vec{x}_1 is independent of c_I and c_Q ³⁴. Furthermore, all elements in \vec{x}_1 have the same sign, which is expected by the Perron-Frobenius theorem for non-positive (or non-negative) matrices. Although all eigenvectors and eigenvalues for the matrix \mathbf{C} are known, to obtain a quantum dragon one only needs the single eigenvector \vec{x}_1 and its associated eigenvalue. Connecting the device based on a rectangular graph to the leads with $\vec{w} = \vec{u} = -\vec{x}_1$ and using the vector \vec{x}_1 for the mapping allows an exact mapping onto a 1D device with the same $\mathcal{T}(E)$. This exact mapping is for any nanodevice based on a rectangular graph for any intra-slice TB parameters ϵ_j and t_j and any inter-slice TB parameters $s_{nn,j}$ and $s_{nnn,j}$. The exact mapping exists whether the lattice can be viewed as planar when all TB parameters are independent of the slice index (as in Fig. 1), or ones which are most likely non-planar when the TB parameters depend on the slice index j , as in Fig. 2.

Now that the exact mapping has been found, the only question to ask is what TB parameters give the mapped 1D system with the same TB parameters as the lead, namely on site energies $\epsilon_{lead} = 0$ and hopping strengths t_{lead} . These systems will be quantum dragons. The eigenvalues of the intra-slice matrices \mathbf{A}_j of Eq. (5) associated with eigenvector \vec{x}_1 have eigenvalues from Eq. (10)

$$\lambda_j = \epsilon_j - 2t_j \cos\left(\frac{\pi}{m+1}\right) \quad \text{for } j = 1, 2, \dots, \ell. \quad (12)$$

Similarly, from Eq. (10) and Eq. (6) the inter-slice matrices $\mathbf{B}_{j,j+1}$ have eigenvalues

$$\eta_j = -s_{nn,j} - 2s_{nnn,j} \cos\left(\frac{\pi}{m+1}\right) \quad (13)$$

for $j = 1, 2, \dots, \ell - 1$. The on site energies of the 1D mapped system are λ_j , and therefore a quantum dragon requires all $\lambda_j = 0$, and hence from Eq. (12)

$$\epsilon_j = 2t_j \cos\left(\frac{\pi}{m+1}\right) \quad \text{for } j = 1, 2, \dots, \ell. \quad (14)$$

The mapped 1D system has hopping parameters between the mapped 1D device atoms equal to η_j , and therefore a quantum dragon requires all $\eta_j = -t_{lead}$, and therefore from Eq. (13)

$$t_{lead} = s_{nn,j} + 2s_{nnn,j} \cos\left(\frac{\pi}{m+1}\right) \quad (15)$$

for all $j = 1, 2, \dots, \ell - 1$. Furthermore, for a quantum dragon the connection vectors must be given by

$$\vec{w} = \vec{u} = -t_{lead}\vec{x}_1. \quad (16)$$

For every slice j the intra-slice nn hopping t_j may be any random value, provided for a quantum dragon the on site energy of slice j satisfies Eq. (14). Similarly for the inter-slice hopping terms $s_{nn,j}$ and $s_{nnn,j}$ may be any random values provided they are correlated to satisfy Eq. (15). Therefore for every value of the index j , Eq. (14) and Eq. (15) define what we mean by correlated randomness.

IV. NUMERICAL CALCULATION OF UNIFORM QUANTUM DRAGONS

Here we provide a numerical example to illustrate the concept of quantum dragons for uniform leads, based on the analysis in the previous section. The nanodevice can be viewed as related to the one in Fig. 2, except for larger m and ℓ values. Our numerical results are shown in Fig. 3.

Any distribution for picking the random TB parameters is allowed. For Fig. 3 the intra-slice terms, t_j , were uniformly distributed between $[0, 2t_{lead}]$ and in this section we set $t_{lead} = 1$. Then we set all m on site energies of the atoms in slice j to be given by Eq. (14). The top

plot in Fig. 3 shows our explicit values for ϵ_j (blue circles) and t_j (orange circles). In order to keep all hopping strengths real and positive, since we are studying devices in zero magnetic field, for the inter-slice TB parameters for every slice j we choose two random numbers $r_{nn,j}$ and $r_{nnn,j}$ uniformly distributed in $[0, 2t_{lead}]$ and then to satisfy Eq. (15) choose the inter-slice hopping strengths to be

$$\begin{aligned} s_{nn,j} &= \frac{r_{nn,j} t_{lead}}{r_{nn,j} + 2r_{nnn,j} \cos\left(\frac{\pi}{m+1}\right)} \\ s_{nnn,j} &= \frac{r_{nnn,j} t_{lead}}{r_{nn,j} + 2r_{nnn,j} \cos\left(\frac{\pi}{m+1}\right)} \end{aligned} \quad (17)$$

with the explicit values used shown in Fig. 3.

In Fig. 3, 251 energies equally distributed between $-1.999 \leq E \leq 1.999$ were calculated. There are singularities present at the lead band edges at $E = \pm 2$, so these were avoided. For every energy E the matrix \mathbf{M}_{256} , with the same structure as the matrix \mathbf{M}_4 in Eq. (4), was numerically inverted. Since $\ell m = 4096$ the matrix \mathbf{M}_{256} is of dimension 4098×4098 . As expected for the quantum dragon system, in Fig. 3 we see $\mathcal{T}(E)=1$ for all E (red circles, which run together so they seem to form a line segment).

We also wanted to see how $\mathcal{T}(E)$ behaves when we move away from the condition of correlated disorder. For uncorrelated disorder, due to Anderson localization^{35,36}, we expect very small $\mathcal{T}(E)$ for almost all energies for a finite device size (finite ℓm). Therefore we also calculated $\mathcal{T}(E)$ for the case where to the on site energy ϵ_j we added a small uncorrelated random value which is different for all ℓm atoms in the nanodevice. Explicitly, we chose a random variate from a normal distribution of mean zero and standard deviation unity, and then multiply by a strength Δ . The same random numbers were used for all values of Δ studied. Note if $\Delta \neq 0$ no exact mapping onto an equivalent 1D system is known. Figure 3 shows results for the three values $\Delta=0$ (a quantum dragon, red points), $\Delta=0.25$ (cyan points), and $\Delta=0.5$ (blue points). As expected for $\Delta \neq 0$ the transmission is almost always small due to Anderson localization, and is typically smaller for larger values of Δ . Note the logarithmic scale in Fig. 3 for $\mathcal{T}(E)$, so the device has become an insulator for $\Delta \neq 0$, while it is a quantum dragon with a perfectly conducting channel for $\Delta=0$.

V. DISCUSSION AND CONCLUSIONS

We have found the quantum dragon property, namely a perfectly conducting channel, $\mathcal{T}(E)=1$, for nanostructures based on rectangular graphs. The graphs have open boundary conditions, with two sides connected to semi-infinite leads. The hopping is nn, and between slices nnn hopping is also included. For no disorder, the graphs become a rectangular crystal, and band structure properties can be determined. When there is strong disorder,

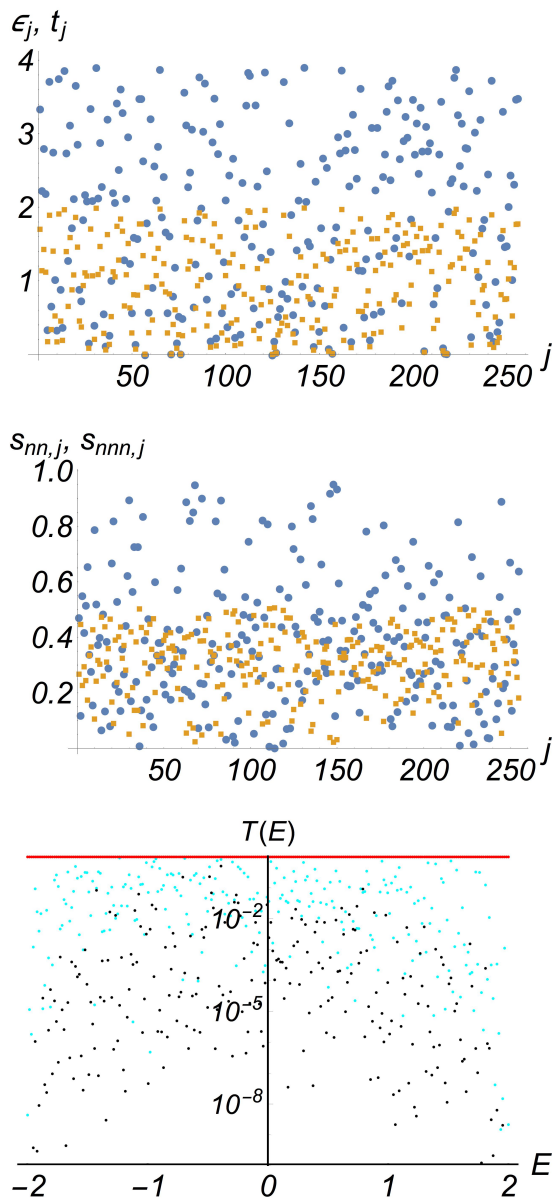


FIG. 3. (Color online.) An example of uniform leads connected to a disordered, rectangular nanodevice with $\ell=256$ and $m=16$. (Top) The correlated random values for slice j for ϵ_j (blue circles) and t_j (orange squares). (Middle) The correlated random values between slices numbered j and $j+1$ for $s_{nn,j}$ (blue circles) and $s_{nnn,j}$ (orange squares). (Bottom) Transmission as a function of energy for the disorder in the two upper graphs (red), showing the quantum dragon condition $\mathcal{T}(E) = 1$. The three values shown are $\Delta=0$ (red) for correlated disorder only, and for added on site uncorrelated disorder of strength $\Delta = 0.25$ (cyan) and $\Delta = 0.5$ (blue).

as in Fig. 2 and Fig. 6, band structure is ill defined. Nevertheless, even though there is arbitrarily strong scattering, $\mathcal{T}(E)=1$ for all energies which propagate through the leads. Hence quantum dragon nanodevices can be based on rectangular graphs. For the quantum dragon nanodevices, because $\mathcal{T}(E)=1$, the electrical conductance will be

$G=G_0$ in two terminal and $G=\infty$ in four terminal measurements. Furthermore, the shot power noise is $P=0$.

The existence of quantum dragon solutions for electron transmission is extremely relevant because of recent experimental single layer thick materials based on rectangular lattices which have been recently synthesized, including monolayers of Fe²⁷ and of CuO^{28,29}.

Future work includes finding quantum dragons for different boundary conditions of the underlying rectangular lattices. Some of these were included in a recent Ph.D. dissertation³⁷. In order to find quantum dragons with strong disorder, the crucial idea is all intra-slice and all inter-slice parts of the Hamiltonian must have a common eigenvector, and furthermore this eigenvector must correspond to a physically realizable connection to the leads. For nanodevices based on rectangular lattices, this is possible for other boundary conditions³⁷. These studies may benefit from renormalization group calculations for transport, such as have been used for hierarchical lattices³⁸.

Other further work could be to study the even-odd structure of rectangular CuO lattices, where experimentally even-numbered and odd-numbered slices have different structures^{28,29}. One expects again quantum dragon solutions, because the same type of even-odd structure was exploited in the study of quantum dragon solutions in single walled carbon nanotubes¹⁹. Further work can also be performed examining quantities such as a local density of states (LDOS). The Green's function $\mathcal{G}(E)$ is given in Eq. (59), and the LDOS at E is the imaginary part of the diagonal elements of $\mathcal{G}(E)$ divided by π ³⁹. For a quantum dragon, as shown in Fig. 4, the correlated disorder of a quantum dragon gives a LDOS independent of the slice index j , even though the disorder on every slice is different.

A further investigation of added disorder near a quantum dragon solution is also warranted. We have observed such an analysis will require the study of the Fano resonances⁴⁰ present, which are a source of the small values for electron transmission seen in Fig. 3 and 7. The full counting statistics of nanodevices⁴² nearby in parameter space to quantum dragon solutions would also be of interest. One could also investigate how such quantum dragon solutions behave if one goes beyond the TB model, for example using an exact discretization of the Schrödinger equation⁴¹, or due to many-electron effects such as were used recently to analyze transport through a nanoscale ring-dot device⁴³.

The possibility of technologically using quantum dragon solutions for field effect transistors or sensors⁴⁴ also deserves further explanation. Furthermore, the possibilities exist related dragon solutions may also be present in other strongly disordered systems, for example where the open boundary conditions and disorder would normally lead to transverse Anderson localization³⁶ in optical waveguides.

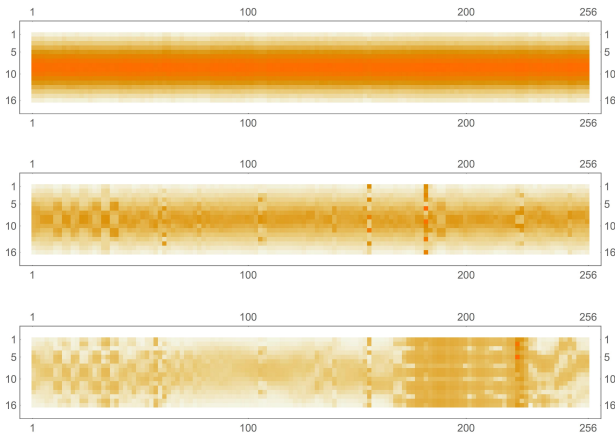


FIG. 4. (Color online.) The local density of states (LDOS) for a strongly disordered nanodevice based on a rectangular lattice with $\ell=256$ and $m=16$, attached to uniform leads. The correlated disorder in the TB parameters ϵ_j , t_j , $s_{nn,j}$, and $s_{nnn,j}$ is similar to Fig. 3. These are calculated with $E=0.01t_{lead}$, but the results are similar for other energies. The color coding has a larger LDOS for brighter, more orange pixels. (Top) The LDOS is independent of the slice j when there is only correlated disorder, so the device is a quantum dragon. Even though there is strong scattering, $\mathcal{T}=1$. (Middle) With added uncorrelated on site disorder of strength $\Delta=0.01$ the LDOS changes dramatically, while the transmission decreases to $\mathcal{T}=0.99851$. (Bottom) The LDOS changes even more when for the same uncorrelated on site random disorder the strength is $\Delta=0.02$, while the transmission has further decreased to $\mathcal{T}=0.98205$.

ACKNOWLEDGEMENTS

One of the authors (MAN) thank Tomáš Novotný and Maciej Maška for useful discussions, and the Faculty of Mathematics and Physics at Charles University in Prague, Czech Republic for hospitality during a stay as a Fulbright Distinguished Chair. Funding for MAN as a Fulbright Distinguished Chair is gratefully acknowledged.

APPENDIX A: FOR FIGURES WITHOUT DISORDER

The complete description of two figures of the device and leads without disorder, namely Fig. 1 and Fig. 5 are given.

1. Figure 1 complete description

An example of the case of uniform (non-dimerized) leads, and no disorder in a rectangular lattice device is shown in Fig. 1. Because of the lack of disorder, the device can be considered to be a planar, rectangular crystal. The location of the device is highlighted in light yellow.

The vertical gray lines show the division into slices, both for the device and for the lead atoms. Here there are $\ell=16$ slices in the device, and $m=7$ atoms in each slice. Therefore, the device has $m\ell=112$ atoms (red spheres). The intra-slice hopping terms are shown by the vertical line segments (green), TB parameters $t_j=t$ for slice j , and are only between nn atoms. The inter-slice hopping terms are for nn interactions shown by the horizontal line segments (red-orange, TB parameter $s_{nn,j}=s_{nn}$), and the nnn interactions shown by the (black, TB parameter $s_{nnn,j}=s_{nnn}$) line segments which form an X-shape. Only four atoms (blue-green) for both the incoming and outgoing semi-infinite leads are shown. The connections between the leads and the device are shown by line segments (cyan) with the width proportional to the elements of the eigenvector \vec{x}_1 in Eq. (11).

2. Figure 5 complete description

Fig. 5 shows an example of the case of dimerized leads and a dimerized device, for no disorder in the rectangular device. Consequently, the device may be considered to be planar. The device is highlighted in light yellow. The vertical gray lines show the division into slices, both for the device and for the lead atoms. Here there are $\ell=4$ slices in the device, and $m=8$ atoms in each slice. Therefore, the device has $m\ell=32$ atoms, denoted by different sized (and colored) spheres for the odd slices (red) and even slices (green). The different colors and sizes represent different values for the TB on site energies ϵ_j . The first (leftmost) slice is numbered one. The intra-slice hopping terms are only between nn atoms, and are shown by the vertical line segments which are thick and green for the odd-numbered slices and thinner and yellow for the even-numbered slices, representing TB parameters t_j . The inter-slice hopping terms are for nn interactions shown by the horizontal line segments (magenta for odd-to-even and yellow for even-to-odd, representing TB parameters $s_{nn,j}$), and the nnn interactions shown by the line segments which form an X-shape (magenta for odd-to-even and black for even-to-odd, representing the TB parameters $s_{nnn,j}$). Only five atoms for the incoming lead and four atoms for the outgoing semi-infinite lead are shown (large and fuchsia colored for odd-numbered atoms, while small and black for even-numbered atoms, representing ϵ_o and ϵ_e TB parameters, respectively). The lead hopping interactions are shown as thick (white) cylinders for odd-to-even hopping terms (representing TB parameters t_{oe}), and thinner (yellow) cylinders for even-to-odd hopping terms (representing TB parameters t_{eo}). The connections between the leads and the device are shown by line segments (cyan for the incoming lead, and magenta for the outgoing lead) with the cylinder width proportional to the elements of the eigenvector \vec{x}_1 in Eq. (11).

APPENDIX B: FIGURES WITH DISORDER

The description for Fig. 2 and Fig. 6 is presented.

Consider a model where atoms in slice j must be the same distance a_j apart, as in a ball-and-stick polymer model. Hence, between nn atoms within slice j there is only a single distance a_j allowed between the atoms (equivalent to attachment of springs with infinite spring constant and equilibrium distance a_j).

Between atoms in two neighboring slices, there are nn and nnn equilibrium spring distances. Let the hard spheres in slice j be of radius R_j . Follow Konishi, et al⁴⁵ for the Monte Carlo simulations and energy functions. The nn elastic interactions are

$$\mathcal{H}_{nn} = \frac{m k_{j,j+1}}{2} (r_{j,j+1} - (R_j + R_{j+1}))^2 \quad (18)$$

since all distances must be the same between the intra-slice nn atoms. Here

$$\begin{aligned} r_{j,j+1} &= \sqrt{(x_{j,i} - x_{j+1,i})^2 + (y_{j,i} - y_{j+1,i})^2} \\ &= \sqrt{\Delta x_j^2 + \Delta y_j^2} \end{aligned} \quad (19)$$

is the distance (with the atoms confined to have the same z value (with the z value the direction along which current will flow). Here the index i labels the m atoms in the slice labeled j . This distance must be the same between nn for all atoms in slices j and $j+1$, and consequently, they must have the same value of Δx_j and Δy_j . Similarly, the nnn elastic term is

$$\mathcal{H}_{nnn} = \frac{2(m-1) \hat{k}_{j,j+1}}{2} \left(\hat{r}_{j,j+1} - \sqrt{2} (R_j + R_{j+1}) \right)^2 \quad (20)$$

with

$$\begin{aligned} \hat{r}_{j,j+1} &= \sqrt{(x_{j,i} - x_{j+1,i\pm 1})^2 + (y_{j,i} - y_{j+1,i\pm 1})^2} \\ &= \sqrt{\Delta \hat{x}_j^2 + \Delta \hat{y}_j^2}. \end{aligned} \quad (21)$$

We assume the hard sphere radii (the radii of the plotted spheres in the figures) is proportional to $|\epsilon_j|$ for slice j , namely $R_j \propto |\epsilon_j|$. We assume the distance between atoms within a slice has $a_j \propto t_j$, with t_j also reflected by the radii of the cylinders representing the intra-slice bonds in the figures. We assume the spring constants between slices have $k_{j,j+1} \propto s_{nn,j}$ and $\hat{k}_{j,j+1} \propto s_{nnn,j}$, and also the width of the cylinders representing the bonds have the same proportionality. One then has a complete (classical) Hamiltonian for the nanosystems we study. The configuration of the classical representation of the nanodevice is then found by performing a simulated annealing Monte Carlo process to attempt to minimize the total elastic energy of the nanodevice.

1. Figure 2 complete description

Figure 2 contains an example of a nanodevice with uniform (non-dimerized) leads. The device has $\ell=20$ slices, and $m=8$ atoms in every slice. The underlying graph is rectangular, with nn interactions and also with nnn interactions between atoms in neighboring slices. Only five atoms in both the incoming and outgoing semi-infinite leads are shown. The radii of the spheres are proportional to $|\epsilon_j|$, and the radii of the cylinders representing the bonds are proportional to the hopping strengths. The bonds are magenta for nnn bonds (TB parameter $s_{nnn,j}$ for slice j), cyan for nn inter-slice bonds (TB $s_{nn,j}$), and green for nn intra-slice bonds (TB t_j). The t_j are different for every slice, and were chosen to be uniformly distributed in $[0, 2t_{lead}]$. The on site energies of slice j are all the same, with the ϵ_j given by the quantum dragon condition of Eq. (14). The inter-slice bonds are also all different, with the $s_{nn,j}$ and $s_{nnn,j}$ chosen to satisfy the quantum dragon condition of Eq. (15). The connections between the leads and the device, blue-green cylinders, have strengths given by Eq. (16). Note the extreme disorder in the system, and that it is very far from a rectangular crystal, rather it is a structure based on a rectangular graph. Nevertheless, for transmission it has $\mathcal{T}(E)=1$.

2. Figure 6 complete description

Figure 6 contains an example of a nanodevice with dimerized leads. The device has $\ell=16$ slices, and $m=7$ atoms in every slice. The underlying graph is rectangular, with nn interactions and also with nnn interactions. Only five atoms in both the incoming and outgoing semi-infinite leads are shown, with different colors and radii reflecting different on site energies, ϵ_o (pink) and ϵ_e (black). The hopping terms in the leads are also dimerized, representing t_{eo} (cyan, thick cylinder, smaller lattice spacing) and t_{oe} (pink, thin cylinder, larger lattice spacing). The radii of the spheres in the nanodevice are proportional to $|\epsilon_j|$, with atoms red for odd-numbered j and black for even-numbered j . The radii of the cylinders representing the bonds are proportional to the hopping strengths. The nnn bonds form an X-shape (TB parameter $s_{nnn,j}$ for slice j , magenta for odd j , cyan for even j). The nn inter-slice bonds, TB $s_{nn,j}$, are also magenta for odd j and cyan for even j . The nn intra-slice bonds, TB t_j , are green for j odd and yellow for j even. The t_j are different for every slice, and were chosen to be uniformly distributed in $[0, 2t_{oe}]$ ($[0, 2t_{eo}]$) for odd (even) j . The on site energies of slice j are all the same, with the ϵ_j given by the quantum dragon condition of Eq. (47). The inter-slice bonds are also all different, with the $s_{nn,j}$ and $s_{nnn,j}$ chosen to satisfy the quantum dragon condition of Eq. (49) and Eq. (50). The connections between the leads and the device, blue-green cylinders, have strengths proportional to \bar{x}_1 with strengths given by the dragon condition in Eq. (45). Note the extreme disorder in the

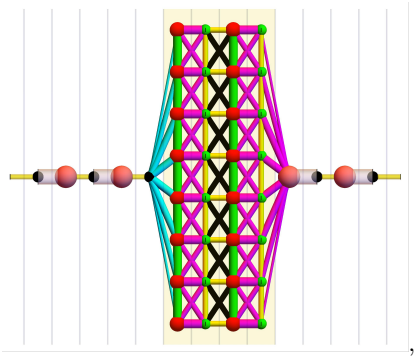


FIG. 5. (Color online.) An example of dimerized leads connected to a dimerized rectangular device, both without disorder. See Appendix A.2 for a complete description.

system, and that it is very far from a rectangular crystal, being rather based on a rectangular graph. Nevertheless, for transmission it is a quantum dragon with $\mathcal{T}(E)=1$ for all energies that propagate in the leads.

APPENDIX C: DERIVATION OF MATRIX METHOD FOR DIMERIZED LEADS

In this appendix, an outline of the derivation for the transmission via the matrix method is given. This par-

The ansatz makes use of Bloch's theorem⁴⁶ through the phase factor δ . Multiplying through by the Hamiltonian of the outgoing lead becomes (corresponding to Eq. [A4] of ref. 19)

$$\begin{aligned} t_T e^{iq(j-1)} [-t_{eo}\delta e^{-iq} + (\epsilon_o - E) - t_{oe}\delta e^{iq}] &= 0 & j = 3, 5, 7, \dots \\ t_T e^{iq(j-1)} [-t_{oe}e^{-iq} + (\epsilon_e - E)\delta - t_{eo}e^{iq}] &= 0 & j = 2, 4, 6, \dots \end{aligned} \quad (23)$$

which can be solved to eliminate δ to give (corresponding to Eq. [A5])

$$\cos(2q) = \frac{(\epsilon_e - E)(\epsilon_o - E) - t_{eo}^2 - t_{oe}^2}{2t_{eo}t_{oe}} \quad (24)$$

and using the double angle formula for $\cos(2q)$ gives

$$\cos(q) = \pm \sqrt{\frac{(\epsilon_e - E)(\epsilon_o - E) - (t_{eo} - t_{oe})^2}{4t_{eo}t_{oe}}} \quad (25)$$

allels Appendix A of ref. 19, with the exception here different on site energies for the dimerized leads are also included. This parallels the case of uniform leads²⁶, which is also derived in the supplemental material of the 2014 quantum dragon paper¹⁹. For uniform leads the matrix form in the main text is obtained from results in this section.

Consider a nanodevice with m atoms in every slice and with ℓ slices, connected to dimerized leads, with an example shown in Fig. 5. The leads (both incoming and outgoing) have on site energy ϵ_e (ϵ_o) for even (odd) numbered sites. The arrangement, including numbering of the lead atoms, is as in the figure in Appendix A of ref. 19. The outgoing lead is first completely analyzed, then the incoming lead is addressed. The traveling-wave ansatz within the outgoing lead is the same as Eq. [A3] of ref. 19 (note equation numbers from the 2014 paper 19 are enclosed in square brackets)

$$\begin{aligned} \psi_j &= t_T e^{iq(j-1)} & j = 1, 3, 5, \dots \\ \psi_j &= t_T \delta e^{iq(j-1)} & j = 2, 4, 6, \dots \end{aligned} \quad (22)$$

corresponding to Eq. [A6]. A propagating wave requires q to be real, and hence $0 \leq \cos(q) \leq 1$ or $-1 \leq \cos(q) \leq 0$ for the two signs in front of the square root in Eq. (25).

One is free to set the zero for energy for the entire system, and a reasonable choice is to set the zero at $(\epsilon_o + \epsilon_e)/2$. This can be accomplished by insisting $\epsilon_o = -\epsilon_e$, with the zero of energy then at zero, which is also the midpoint between ϵ_o and ϵ_e . This gives propagating waves (corresponding to Eq. [A7]) for positive energies of

$$\sqrt{\left(\frac{\epsilon_e - \epsilon_o}{2}\right)^2 + (t_{eo} - t_{oe})^2} \leq E \leq \sqrt{\left(\frac{\epsilon_e - \epsilon_o}{2}\right)^2 + (t_{eo} + t_{oe})^2} \quad (26)$$

and

$$-\sqrt{\left(\frac{\epsilon_e - \epsilon_o}{2}\right)^2 + (t_{eo} + t_{oe})^2} \leq E \leq -\sqrt{\left(\frac{\epsilon_e - \epsilon_o}{2}\right)^2 + (t_{eo} - t_{oe})^2} \quad (27)$$

for negative energies. By manipulating the two expressions in Eq. (23) one finds

$$\begin{aligned}\delta &= \frac{\epsilon_o - E}{\frac{t_{oe}e^{iq} + t_{eo}e^{-iq}}{t_{eo}e^{iq} + t_{oe}e^{-iq}}} \\ &= \frac{\epsilon_o - E}{\epsilon_e - E}\end{aligned}\quad (28)$$

corresponding to Eq. [A8]. One also finds using the outgoing lead equations as in Eq. [A10]

$$\begin{aligned}\xi_u &= \epsilon_o - E - t_{oe}\delta e^{iq} \\ &= (\epsilon_o - E) \left(1 - t_{oe} \frac{e^{iq}}{t_{oe}e^{iq} + t_{eo}e^{-iq}} \right) \\ &= (\epsilon_o - E) \frac{t_{eo}e^{-iq}}{t_{oe}e^{iq} + t_{eo}e^{-iq}}\end{aligned}\quad (29)$$

$$\begin{aligned}e^{-iqj} [\epsilon_o - E - t_{eo}\delta e^{-iq} - t_{oe}\delta e^{iq}] + r e^{iqj} [\epsilon_o - E - t_{eo}\delta^* e^{iq} - t_{oe}\delta^* e^{-iq}] &= 0 & j = 1, 3, 5, \dots \\ e^{-iqj} [\delta(\epsilon_e - E) - t_{oe}e^{-iq} - t_{eo}e^{iq}] + r e^{iqj} [\delta^*(\epsilon_e - E) - t_{oe}e^{iq} - t_{eo}e^{-iq}] &= 0 & j = 2, 4, 6, \dots\end{aligned}\quad (30)$$

which has all four terms in square brackets zero for the expressions for δ in Eq. (28). When $\epsilon_o \neq \epsilon_e$, the values of ξ are different for the incoming (ξ_w) and outgoing (ξ_u) leads. The incoming lead requires the association

$$\begin{aligned}\xi_w &= \epsilon_e - E - \frac{1}{\delta^*} t_{oe} e^{iq} \\ &= (\epsilon_e - E) \frac{t_{eo}e^{-iq}}{t_{oe}e^{iq} + t_{eo}e^{-iq}}\end{aligned}\quad (31)$$

corresponding to Eq. [A12].

For the incoming lead one obtains via the traveling-wave ansatz

$$\begin{aligned}\Lambda &= \xi_w \delta - (\epsilon_e - E) \delta + t_{oe} e^{-iq} \\ &= -t_{oe} \left(\frac{\delta}{\delta^*} e^{iq} - e^{-iq} \right).\end{aligned}\quad (32)$$

Consequently, one obtains the solution to the transmission $\mathcal{T} = |t_T|^2$ from the solution to the matrix equation of the form (written for $\ell=4$)

$$\mathbf{M}_4 \begin{pmatrix} \delta + r\delta^* \\ \vec{\psi}_1 \\ \vec{\psi}_2 \\ \vec{\psi}_3 \\ \vec{\psi}_4 \\ t_T \end{pmatrix} = \begin{pmatrix} \xi_w & \vec{w}^\dagger & \vec{0}^\dagger & \vec{0}^\dagger & \vec{0}^\dagger & 0 \\ \vec{w} & \mathbf{F}_1 & \mathbf{B}_{12} & \mathbf{0} & \mathbf{0} & \vec{0} \\ \vec{0} & \mathbf{B}_{12}^\dagger & \mathbf{F}_2 & \mathbf{B}_{23} & \mathbf{0} & \vec{0} \\ \vec{0} & \mathbf{0} & \mathbf{B}_{23}^\dagger & \mathbf{F}_3 & \mathbf{B}_{34} & \vec{0} \\ \vec{0} & \mathbf{0} & \mathbf{0} & \mathbf{B}_{34}^\dagger & \mathbf{F}_4 & \vec{u} \\ 0 & \vec{0}^\dagger & \vec{0}^\dagger & \vec{0}^\dagger & \vec{u}^\dagger & \xi_u \end{pmatrix} \begin{pmatrix} \delta + r\delta^* \\ \vec{\psi}_1 \\ \vec{\psi}_2 \\ \vec{\psi}_3 \\ \vec{\psi}_4 \\ t_T \end{pmatrix} = \begin{pmatrix} \Lambda \\ \vec{0} \\ \vec{0} \\ \vec{0} \\ \vec{0} \\ 0 \end{pmatrix}\quad (33)$$

corresponding to Eq. [A11]. If $\epsilon_e = \epsilon_o$ one has $\xi_w = \xi_u = \xi$, and therefore obtain the specialized case of Eq. (4). The transmission is calculated by inverting the matrix \mathbf{M}_ℓ for a specific energy, and thereby obtaining $\mathcal{T} = |t_T|^2$.

For dimerized leads with $\epsilon_o = \epsilon_e = 0$ and $t_{eo} \neq t_{oe}$, δ has the form from Eq. [A8] and consequently the energy range of propagating electrons is expressed as Eq. [A7]. For the case of uniform leads, with $\epsilon_o = \epsilon_e = 0$ and $t_{eo} = t_{oe} = t_{lead}$ one has $\delta = 1$,

$$\xi_w = \xi_u = \xi = e^{-iq} = \frac{-E - i\sqrt{4t_{lead}^2 - E^2}}{2t_{lead}}\quad (34)$$

and $\Lambda = -2i \sin(q)$ with electrons of energy $-2t_{lead} \leq E \leq 2t_{lead}$ propagating as in refs. 19, 26, 31, and 32.

with the further definition

APPENDIX D: QUANTUM DRAGONS WITH DIMERIZED LEADS

In this appendix, the exact mapping as well as the locating of quantum dragons is derived for the case of dimerized leads. We assume an underlying rectangular graph with atoms placed on the nodes, and the graph is composed of ℓ slices each of which have m atoms. An example for a rectangular crystal is shown in Fig. 5, and an example based on an underlying rectangular graph, but with strong correlated disorder is shown in Fig. 6.

The intra-slice parts of the device Hamiltonian, \mathbf{A}_j are defined in Eq. (5). The inter-slice parts of the device Hamiltonian, $\mathbf{B}_{j,j+1}$, are defined in Eq. (6). For our nanosystem based on an underlying rectangular graph, all \mathbf{A}_j and $\mathbf{B}_{j,j+1}$ are a sum of a constant times the $m \times m$ identity matrix plus another constant times the matrix

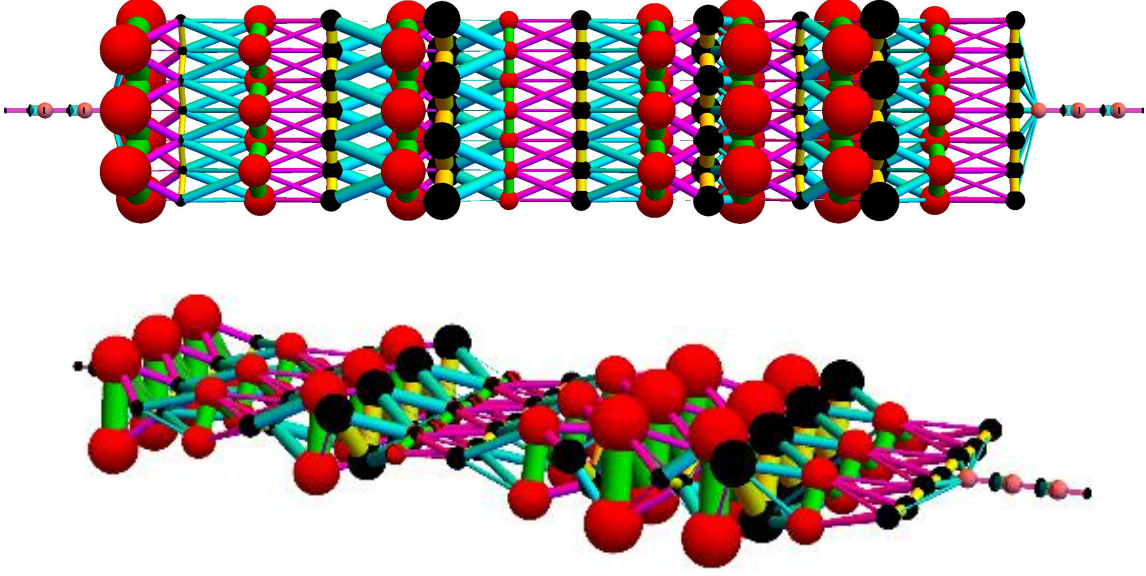


FIG. 6. (Color online.) An example of dimerized leads connected to a dimerized, disordered, rectangular device. The same device is shown in the top (top view) and bottom (oblique view) of the figure. See Appendix B for a complete description.

\mathbf{Q} defined in Eq. (7). The mutual eigenvector of all \mathbf{A}_j and $\mathbf{B}_{j,j+1}$ is the vector \vec{x}_1 defined in Eq. (11).

Define a $m \times m$ transformation matrix

$$\begin{aligned} \mathbf{X} &= (\vec{x}_1 \ \mathbf{Y}_{\text{other}}) \\ \text{and} \\ \mathbf{X}^\dagger &= \begin{pmatrix} \vec{x}_1^\dagger \\ \mathbf{Y}_{\text{other}}^\dagger \end{pmatrix} \end{aligned} \quad (35)$$

where $\mathbf{Y}_{\text{other}}$ is a $m \times (m-1)$ matrix, which can be thought of as being composed of $m-1$ normalized vectors which are orthogonal to \vec{x}_1 and also are orthogonal to each other. Therefore $\mathbf{Y}_{\text{other}}^\dagger \vec{x}_1 = \vec{0}_{m-1}$ and

$\mathbf{Y}^\dagger \mathbf{Y} = \mathbf{I}_{m-1}$. Furthermore,

$$\begin{aligned} \mathbf{X}^\dagger \mathbf{X} &= \begin{pmatrix} \vec{x}_1^\dagger \\ \mathbf{Y}_{\text{other}}^\dagger \end{pmatrix} (\vec{x}_1 \ \mathbf{Y}_{\text{other}}) \\ &= \begin{pmatrix} \vec{x}_1^\dagger \cdot \vec{x}_1 & \vec{x}_1^\dagger \mathbf{Y}_{\text{other}} \\ \mathbf{Y}_{\text{other}}^\dagger \vec{x}_1 & \mathbf{Y}_{\text{other}}^\dagger \mathbf{Y}_{\text{other}} \end{pmatrix} \\ &= \begin{pmatrix} 1 & \vec{0}_{m-1}^\dagger \\ \vec{0}_{m-1} & \mathbf{I}_{m-1} \end{pmatrix} \end{aligned} \quad (36)$$

so $\mathbf{X}^\dagger \mathbf{X} = \mathbf{X} \mathbf{X}^\dagger = \mathbf{I}$.

Next define a $(\ell m + 2) \times (\ell m + 2)$ transformation matrix \mathbf{Z}_ℓ of the form (written for $\ell=4$)

$$\mathbf{Z}_4 = \begin{pmatrix} 1 & \vec{0}^\dagger & \vec{0}^\dagger & \vec{0}^\dagger & \vec{0}^\dagger & 0 \\ \vec{0} & \mathbf{X} & \mathbf{0} & \mathbf{0} & \mathbf{0} & \vec{0} \\ \vec{0} & \mathbf{0} & \mathbf{X} & \mathbf{0} & \mathbf{0} & \vec{0} \\ \vec{0} & \mathbf{0} & \mathbf{0} & \mathbf{X} & \mathbf{0} & \vec{0} \\ \vec{0} & \mathbf{0} & \mathbf{0} & \mathbf{0} & \mathbf{X} & \vec{0} \\ 0 & \vec{0}^\dagger & \vec{0}^\dagger & \vec{0}^\dagger & \vec{0}^\dagger & 1 \end{pmatrix} \quad (37)$$

which has the property $\mathbf{Z}^\dagger \mathbf{Z} = \mathbf{Z} \mathbf{Z}^\dagger = \mathbf{I}$. Multiply the equations of the form of Eq. (33) on the right by \mathbf{Z}_ℓ^\dagger , and also insert the identity $\mathbf{I} = \mathbf{Z}_\ell \mathbf{Z}_\ell^\dagger$ between the matrix \mathbf{M}_ℓ and the vector containing the wavefunctions at each site in the nanodevice. Written for $\ell=4$, this gives

$$\mathbf{Z}_4^\dagger \mathbf{M}_4 \mathbf{Z}_4 \mathbf{Z}_4^\dagger \begin{pmatrix} \delta + r\delta^* \\ \vec{\psi}_1 \\ \vec{\psi}_2 \\ \vec{\psi}_3 \\ \vec{\psi}_4 \\ t_T \end{pmatrix} = \begin{pmatrix} \xi_w & \vec{w}^\dagger \mathbf{X} & \vec{0}^\dagger & \vec{0}^\dagger & \vec{0}^\dagger & 0 \\ \mathbf{X}^\dagger \vec{w} & \mathbf{X}^\dagger \mathbf{F}_1 \mathbf{X} & \mathbf{X}^\dagger \mathbf{B}_{12} \mathbf{X} & \mathbf{0} & \mathbf{0} & \vec{0} \\ \vec{0} & \mathbf{X}^\dagger \mathbf{B}_{12}^\dagger \mathbf{X} & \mathbf{X}^\dagger \mathbf{F}_2 \mathbf{X} & \mathbf{X}^\dagger \mathbf{B}_{23} \mathbf{X} & \mathbf{0} & \vec{0} \\ \vec{0} & \mathbf{0} & \mathbf{X}^\dagger \mathbf{B}_{23}^\dagger \mathbf{X} & \mathbf{X}^\dagger \mathbf{F}_3 \mathbf{X} & \mathbf{X}^\dagger \mathbf{B}_{34} \mathbf{X} & \vec{0} \\ \vec{0} & \mathbf{0} & \mathbf{0} & \mathbf{X}^\dagger \mathbf{B}_{34}^\dagger \mathbf{X} & \mathbf{X}^\dagger \mathbf{F}_4 \mathbf{X} & \mathbf{X}^\dagger \vec{u} \\ 0 & \vec{0}^\dagger & \vec{0}^\dagger & \vec{0}^\dagger & \vec{u}^\dagger \mathbf{X} & \xi_u \end{pmatrix} \begin{pmatrix} \delta + r\delta^* \\ \mathbf{X}^\dagger \vec{\psi}_1 \\ \mathbf{X}^\dagger \vec{\psi}_2 \\ \mathbf{X}^\dagger \vec{\psi}_3 \\ \mathbf{X}^\dagger \vec{\psi}_4 \\ t_T \end{pmatrix} = \mathbf{Z}_4^\dagger \begin{pmatrix} \Lambda \\ \vec{0} \\ \vec{0} \\ \vec{0} \\ \vec{0} \\ 0 \end{pmatrix} = \begin{pmatrix} \Lambda \\ \vec{0} \\ \vec{0} \\ \vec{0} \\ \vec{0} \\ 0 \end{pmatrix}. \quad (38)$$

Because \vec{x}_1 is an eigenvector of all $\mathbf{B}_{j,j+1}$ with eigenvalue η_j in Eq. (13)

$$\mathbf{X}^\dagger \mathbf{B}_{j,j+1} \mathbf{X} = \begin{pmatrix} \eta_j & \vec{0}^\dagger \\ \vec{0} & \tilde{\mathbf{B}}_{j,j+1} \end{pmatrix} = \begin{pmatrix} -\tilde{s}_j & \vec{0}^\dagger \\ \vec{0} & \tilde{\mathbf{B}}_{j,j+1} \end{pmatrix} \quad (39)$$

for some $(m-1) \times (m-1)$ matrix $\tilde{\mathbf{B}}_{j,j+1}$ which will not enter into the calculation of \mathcal{T} . Note we have defined $\tilde{s}_j = -\eta_j$. Similarly, from Eq. (12) and $\mathbf{F}_j = \mathbf{A}_j - E\mathbf{I}$ because \vec{x}_1 is an eigenvector of all \mathbf{A}_j , with eigenvalue λ_j , one has

$$\mathbf{X}^\dagger \mathbf{F}_j \mathbf{X} = \begin{pmatrix} \tilde{\kappa}_j & \vec{0}^\dagger \\ \vec{0} & \tilde{\mathbf{F}}_j \end{pmatrix} \quad (40)$$

with $\tilde{\kappa}_j = \lambda_j - E$ and where $\tilde{\mathbf{F}}_j$ is some $(m-1) \times (m-1)$ matrix which will not enter into the calculation of \mathcal{T} .

We also choose the connections to the nanodevice to be proportional to \vec{x}_1 , so

$$\begin{aligned} \mathbf{X}^\dagger \vec{w} &= -t_w \mathbf{X} \vec{x}_1 = \begin{pmatrix} -t_w \\ 0 \\ \vdots \\ 0 \end{pmatrix} \\ \mathbf{X}^\dagger \vec{u} &= -t_u \mathbf{X} \vec{x}_1 = \begin{pmatrix} -t_u \\ 0 \\ \vdots \\ 0 \end{pmatrix} \end{aligned} \quad (41)$$

for some proportionality constants we label as t_w and t_u .

From Eq. (33) we can calculate the transmission $\mathcal{T} = |t_T|^2$ from the inverse of the $(\ell m + 2) \times (\ell m + 2)$ matrix \mathbf{M}_ℓ as

$$\begin{pmatrix} \delta + r\delta^* \\ \vec{\psi}_1 \\ \vdots \\ \vec{\psi}_\ell \\ t_T \end{pmatrix} = \mathbf{M}_\ell^{-1} \begin{pmatrix} \Lambda \\ \vec{0} \\ \vdots \\ \vec{0} \\ 0 \end{pmatrix}. \quad (42)$$

$$\tilde{\kappa}_j = \lambda_j - E = \epsilon_j - 2t_j \cos\left(\frac{\pi}{m+1}\right) - E = \begin{cases} \epsilon_o - E & j \text{ odd} \\ \epsilon_e - E & j \text{ even} \end{cases} \quad (46)$$

However, with the transformation in Eq. (38) a large part of the matrix is decoupled from both leads, namely the parts which were labeled $\tilde{\mathbf{F}}_j$ and $\tilde{\mathbf{B}}_{j,j+1}$. Therefore, we can also obtain the same transmission $\mathcal{T} = |t_T|^2$ from the inverse of the $(\ell+2) \times (\ell+2)$ matrix $\tilde{\mathbf{M}}_\ell$, which written for $\ell=4$ is

$$\begin{pmatrix} \delta + r\delta^* \\ \vec{\psi}_1 \\ \vdots \\ \vec{\psi}_\ell \\ t_T \end{pmatrix} = \tilde{\mathbf{M}}_\ell^{-1} \begin{pmatrix} \Lambda \\ 0 \\ \vdots \\ 0 \\ 0 \end{pmatrix} \quad (43)$$

where

$$\tilde{\mathbf{M}}_\ell = \begin{pmatrix} \xi_w & -t_w & 0 & \cdots & 0 & 0 & 0 \\ -t_w & \tilde{\kappa}_1 & -\tilde{s}_1 & & 0 & 0 & 0 \\ 0 & -\tilde{s}_1 & \tilde{\kappa}_2 & & 0 & 0 & 0 \\ \vdots & & & \ddots & & & \vdots \\ 0 & 0 & 0 & & \tilde{\kappa}_{\ell-1} & -\tilde{s}_{\ell-1} & 0 \\ 0 & 0 & 0 & & -\tilde{s}_{\ell-1} & \tilde{\kappa}_\ell & -t_u \\ 0 & 0 & 0 & \cdots & 0 & -t_u & \xi_u \end{pmatrix}. \quad (44)$$

Eq. (44) is just the solution of a 1D chain of ℓ atoms with on site energy $\tilde{\kappa}_j + E = \lambda_j$ and nn (inter-slice) hopping strengths \tilde{s}_j . Both the 2D system in Eq. (42) and the 1D system in Eq. (44) have the same transmission $\mathcal{T}(E)$ for all energies E which propagate through the semi-infinite leads. We have therefore completed our exact mapping for the case of dimerized leads.

In order to find a quantum dragon, we need to find TB parameters which turn the equivalent 1D mapped system of Eq. (44) into a portion of length ℓ of the semi-infinite leads. This can be accomplished by insisting that the original 2D device had TB parameters such that after mapping we have the quantum dragon condition for the connections

$$t_w = t_u = t_{eo} \quad (45)$$

where t_{eo} is the hopping strength in the leads from even-numbered to odd-numbered atoms. The quantum dragon conditions for the intra-slice parts of the Hamiltonian are

for $j = 1, 2, \dots, \ell$. This can be satisfied by choosing the t_j at random from any distribution (keeping $t_j > 0$), and then adjusting

$$\epsilon_j = \begin{cases} \epsilon_0 + 2t_j \cos\left(\frac{\pi}{m+1}\right) & j \text{ odd} \\ \epsilon_e + 2t_j \cos\left(\frac{\pi}{m+1}\right) & j \text{ even} \end{cases} \quad (47)$$

which works since ϵ_j can be of either sign. Therefore, the intra-slice nn hopping strength t_j can be any random value, provided one insists the ϵ_j satisfy Eq. (47). For the inter-slice terms of the Hamiltonian, the quantum dragon condition becomes

$$\tilde{s}_j = -\eta_j = s_{nn,j} + 2s_{nnn,j} \cos\left(\frac{\pi}{m+1}\right) = \begin{cases} t_{oe} & j \text{ odd} \\ t_{eo} & j \text{ even} \end{cases} \quad (48)$$

for $j = 1, 2, \dots, \ell - 1$. However, we want to keep the tuned values of $s_{nn,j}$ and $s_{nnn,j}$ both positive, and remember both t_{oe} and t_{eo} are positive. The negative signs for the hopping terms have been put into the calculation by hand. This can be accomplished by for each $j = 1, 2, \dots, \ell - 1$ choosing two random non-negative numbers $r_{nn,j}$ and $r_{nnn,j}$, and setting the 2D device hopping to be

$$\begin{aligned} s_{nn,j} &= \frac{r_{nn,j} t_{oe}}{r_{nn,j} + 2r_{nnn,j} \cos\left(\frac{\pi}{m+1}\right)} \\ s_{nnn,j} &= \frac{r_{nnn,j} t_{oe}}{r_{nn,j} + 2r_{nnn,j} \cos\left(\frac{\pi}{m+1}\right)} \end{aligned} \quad (49)$$

for j odd and

$$\begin{aligned} s_{nn,j} &= \frac{r_{nn,j} t_{eo}}{r_{nn,j} + 2r_{nnn,j} \cos\left(\frac{\pi}{m+1}\right)} \\ s_{nnn,j} &= \frac{r_{nnn,j} t_{eo}}{r_{nn,j} + 2r_{nnn,j} \cos\left(\frac{\pi}{m+1}\right)} \end{aligned} \quad (50)$$

for j even. This completes the quantum dragon conditions, which when satisfied gives $\mathcal{T}(E)=1$ for all energies which propagate through the leads.

Fig. 7 is an example of a quantum dragon with dimerized leads and a dimerized device. The device has $\ell=500$ slices each with $m=7$ atoms. The leads have $t_{eo}=0.8$ and $t_{oe}=1.2$ together with lead on site energies $\epsilon_o=-0.3$ and $\epsilon_e=0.3$ (remember we have set our zero of energy at the midpoint between the on site energies of the even and odd numbered leads). For these leads, from Eq. (26) and (27), the leads allow electron transmission for energies in the ranges $-\frac{\sqrt{409}}{10} \leq E \leq -\frac{1}{2}$ and $\frac{1}{2} \leq E \leq \frac{\sqrt{409}}{10} \approx 2.02237$. Only the positive energy range is shown in Fig. 7. Although any distribution of intra-slice hopping could be used, here the t_j were chosen uniformly in $[0, 2t_{eo}]$ for even numbered slices and in $[0, 2t_{oe}]$ in odd numbered slices. Then the on site energy was set to the quantum dragon condition in Eq. (47). Similarly for the inter-slice hopping the $s_{nn,j}$ and $s_{nnn,j}$ were taken to be uniformly distributed in $[0, 2t_{eo}]$ for even j and in $[0, 2t_{oe}]$ for odd j , and then tuned to the quantum dragon conditions as in Eq. (49) for j odd and Eq. (50) for j even. A total of

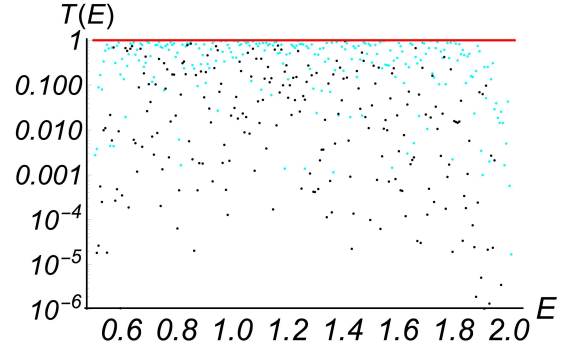


FIG. 7. (Color online.) An example of dimerized leads connected to a disordered, rectangular nanodevice with $\ell=500$ and $m=7$. Transmission as a function of energy for the correlated disorder (red), showing the quantum dragon condition $\mathcal{T}(E) = 1$. The three values shown have uncorrelated disorder so $\Delta = 0$ (red dots), and added on site uncorrelated disorder of strength $\Delta=0.05$ (cyan dots) and $\Delta=0.10$ (blue dots). See the text for a full description.

251 different energies uniformly spaced between 0.50001 and 2.0223 were calculated. Figure 7 shows for the quantum dragon condition for the TB parameters all energies have $\mathcal{T}(E) = 1$ (red dots, which overlap to look like a line segment). Additional uncorrelated random disorder was also included, every site having a different on site added disorder found by choosing a random variant from a normal distribution of mean zero and standard deviation unity, and then multiplying by a value Δ . Figure 7 also shows the, usually very small, values for $\mathcal{T}(E)$ obtained for $\Delta=0.05$ (cyan dots) and $\Delta=0.10$ (blue dots).

APPENDIX E: RELATIONSHIP BETWEEN MATRIX AND GREEN'S FUNCTION METHODS

The relationship for dimerized single-channel leads, between the traditional Green's function method^{4-9,33} of solution and the matrix method of solution of the time-independent Schrödinger equation is presented. The leads have possibility for dimerized hopping (t_{eo} and t_{oe})

and dimerized on site energies (ϵ_e and ϵ_o).

The matrix method for dimerized leads, related to Eq. (4), has the general form

$$\begin{pmatrix} \xi_w & \vec{w}^\dagger & 0 \\ \vec{w} & \mathcal{H} - E\mathbf{I} & \vec{u} \\ 0 & \vec{u}^\dagger & \xi_u \end{pmatrix} \begin{pmatrix} \delta + r\delta^* \\ \vec{\psi} \\ t_T \end{pmatrix} = \begin{pmatrix} \Lambda \\ \vec{0} \\ 0 \end{pmatrix} \quad (51)$$

and requires one to find the inverse of the matrix in or-

$$\begin{pmatrix} \xi_w^{-1} + \xi_w^{-2}\vec{w}^\dagger\mathbf{L}\vec{w} & -\xi_w^{-1}\vec{w}^\dagger\mathbf{L} & \xi_w^{-1}\xi_u^{-1}\vec{w}^\dagger\mathbf{L}\vec{u} \\ -\xi_w^{-1}\mathbf{L}\vec{w} & \mathbf{L} & -\xi_u^{-1}\mathbf{L}\vec{u} \\ \xi_w^{-1}\xi_u^{-1}\vec{u}^\dagger\mathbf{L}\vec{w} & -\xi_u^{-1}\vec{u}^\dagger\mathbf{L} & \xi_u^{-1} + \xi_u^{-2}\vec{u}^\dagger\mathbf{L}\vec{u} \end{pmatrix} \begin{pmatrix} \xi_w & \vec{w}^\dagger & 0 \\ \vec{w} & \mathcal{H} - E\mathbf{I} & \vec{u} \\ 0 & \vec{u}^\dagger & \xi_u \end{pmatrix} = \begin{pmatrix} 1 & \vec{0}^\dagger & 0 \\ \vec{0} & \mathbf{I} & \vec{0} \\ 0 & \vec{0}^\dagger & 1 \end{pmatrix} \quad (52)$$

with the definition

$$\mathbf{L} = [\mathcal{H} - E\mathbf{I} - \xi_w^{-1}\vec{w}\vec{w}^\dagger - \xi_u^{-1}\vec{u}\vec{u}^\dagger]^{-1}. \quad (53)$$

This gives $\mathbf{L}(\mathcal{H} - E\mathbf{I}) = \mathbf{I} + \xi_w^{-1}\mathbf{L}\vec{w}\vec{w}^\dagger + \xi_u^{-1}\mathbf{L}\vec{u}\vec{u}^\dagger$, which is useful in showing Eq. (52). Therefore, we have calculated the inverse of the matrix in Eq. (51), namely the matrix on the left in Eq. (52).

Multiplying through in Eq. (51) by the matrix inverse, one obtains

$$\begin{pmatrix} \delta + r\delta^* \\ \vec{\psi} \\ t_T \end{pmatrix} = \Lambda \xi_w^{-1} \begin{pmatrix} 1 + \xi_w^{-1}\vec{w}^\dagger\mathbf{L}\vec{w} \\ -\mathbf{L}\vec{w} \\ \xi_u^{-1}\vec{u}^\dagger\mathbf{L}\vec{w} \end{pmatrix} \quad (54)$$

and consequently the transmission is

$$\mathcal{T}(E) = |t_T|^2 = |\Lambda|^2 |\xi_w^{-1}|^2 |\xi_u^{-1}|^2 |\vec{u}^\dagger\mathbf{L}\vec{w}|^2. \quad (55)$$

In the case of uniform leads the on site energies ϵ_e and ϵ_o are set to zero, giving the zero of energy. Furthermore, for uniform leads $t_{eo} = t_{oe} = 1$, setting the unit of energy. Then $\xi_w = \xi_u = \xi$ and $\xi^{-1} = \xi^*$ and $|\xi^{-1}|^2 = 1$, as well as $\Lambda = -2i \sin(q)$, giving the transmission

$$\mathcal{T}(E) = |t_T|^2 = 4 \sin^2(q) |\vec{u}^\dagger\mathbf{L}\vec{w}|^2. \quad (56)$$

In the Green's function formalism^{4-9,33}, for the dimerized leads, the self-energy matrix for the incoming lead is

$$\Sigma_1 = -\xi_w^{-1}\vec{w}\vec{w}^\dagger \quad (57)$$

and for the outgoing lead

$$\Sigma_2 = -\xi_u^{-1}\vec{u}\vec{u}^\dagger \quad (58)$$

and the Green's function is

$$\begin{aligned} \mathcal{G} &= -\mathbf{L} \\ &= -[\mathcal{H} - E\mathbf{I} - \xi_w^{-1}\vec{w}\vec{w}^\dagger - \xi_u^{-1}\vec{u}\vec{u}^\dagger]^{-1} \\ &= (E\mathbf{I} - \mathcal{H} - \Sigma_1 - \Sigma_2)^{-1}. \end{aligned} \quad (59)$$

der to find t_T . The transmission for any E is then easily calculated by $\mathcal{T} = |t_T|^2$. The matrix in Eq. (51) is not Hermitian, even for uniform leads due to the ξ_w and ξ_u factors. The matrix \mathcal{H} is the Hamiltonian of the nanodevice, and is therefore Hermitian.

Any block-tridiagonal matrix of the form above has an inverse matrix that can easily be written as

Furthermore, since $\vec{u}^\dagger\mathbf{L}\vec{w}$ is a number, one can use $(\vec{u}^\dagger\mathbf{L}\vec{w})^* = (\vec{u}^\dagger\mathbf{L}\vec{w})^\dagger = \vec{w}^\dagger\mathbf{L}^\dagger\vec{u}$ to obtain

$$\begin{aligned} |\vec{u}^\dagger\mathbf{L}\vec{w}|^2 &= \vec{u}^\dagger\mathbf{L}\vec{w} (\vec{u}^\dagger\mathbf{L}\vec{w})^* \\ &= \vec{u}^\dagger\mathbf{L}\vec{w}\vec{w}^\dagger\mathbf{L}^\dagger\vec{u} \\ &= \text{Tr}(\vec{u}^\dagger\mathbf{L}\vec{w}\vec{w}^\dagger\mathbf{L}^\dagger\vec{u}) \\ &= \text{Tr}(\mathbf{L}\vec{w}\vec{w}^\dagger\mathbf{L}^\dagger\vec{u}\vec{u}^\dagger) \\ &= \text{Tr}(\mathcal{G}\vec{w}\vec{w}^\dagger\mathcal{G}^\dagger\vec{u}\vec{u}^\dagger) \end{aligned} \quad (60)$$

where $\text{Tr}(\cdot)$ is the trace of the matrix, and the cyclic property of matrices within the trace have been used.

In the normal fashion for Green's function calculations^{4-9,33}, this gives for both dimerized and uniform leads

$$\begin{aligned} \Gamma_1 &= i(\Sigma_1 - \Sigma_1^\dagger) \\ &= -i \left[\xi_w^{-1} - (\xi_w^{-1})^* \right] \vec{w}\vec{w}^\dagger \\ &= -i \left[\frac{t_{oe}e^{iq} + t_{eo}e^{-iq}}{t_{eo}(\epsilon_e - E)e^{-iq}} - \frac{t_{oe}e^{-iq} + t_{eo}e^{iq}}{t_{eo}(\epsilon_e - E)e^{iq}} \right] \vec{w}\vec{w}^\dagger \\ &= -i \left[\frac{t_{oe}e^{2iq} + t_{eo}e^{-2iq} - t_{eo}}{t_{eo}(\epsilon_e - E)e^{iq}e^{-iq}} \right] \vec{w}\vec{w}^\dagger \\ &= -i \left[\frac{t_{oe}(2i) \left(\frac{e^{2iq} - e^{-2iq}}{2i} \right)}{t_{eo}(\epsilon_e - E)} \right] \vec{w}\vec{w}^\dagger \\ &= \frac{2t_{oe}}{t_{eo}(\epsilon_e - E)} \sin(2q) \vec{w}\vec{w}^\dagger \\ &= \gamma_1 \vec{w}\vec{w}^\dagger \end{aligned} \quad (61)$$

and similarly

$$\begin{aligned} \Gamma_2 &= i(\Sigma_2 - \Sigma_2^\dagger) \\ &= -i \left[\xi_u^{-1} - (\xi_u^{-1})^* \right] \vec{u}\vec{u}^\dagger \\ &= -i \left[\frac{t_{oe}e^{iq} + t_{eo}e^{-iq}}{t_{eo}(\epsilon_o - E)e^{-iq}} - \frac{t_{oe}e^{-iq} + t_{eo}e^{iq}}{t_{eo}(\epsilon_o - E)e^{iq}} \right] \vec{u}\vec{u}^\dagger \\ &= -i \left[\frac{t_{oe}e^{2iq} + t_{eo}e^{-2iq} - t_{eo}}{t_{eo}(\epsilon_o - E)e^{iq}e^{-iq}} \right] \vec{u}\vec{u}^\dagger \\ &= -i \left[\frac{t_{oe}(2i) \left(\frac{e^{2iq} - e^{-2iq}}{2i} \right)}{t_{eo}(\epsilon_o - E)} \right] \vec{u}\vec{u}^\dagger \\ &= \frac{2t_{oe}}{t_{eo}(\epsilon_o - E)} \sin(2q) \vec{u}\vec{u}^\dagger \\ &= \gamma_2 \vec{u}\vec{u}^\dagger \end{aligned} \quad (62)$$

which defines γ_1 and γ_2 .

Therefore, we only need to show to complete the equiv-

alence between the Green's function and matrix methods that $|\xi_w^{-1}|^2 |\xi_u^{-1}|^2 \Lambda \Lambda^* = \gamma_1 \gamma_2^*$. This is shown via

$$\begin{aligned}
|\xi_w^{-1}|^2 |\xi_u^{-1}|^2 &= \frac{(t_{oe} e^{iq} + t_{eo} e^{-iq})(t_{oe} e^{-iq} + t_{eo} e^{iq})}{t_{eo}^2 (\epsilon_e - E)^2} \frac{(t_{oe} e^{iq} + t_{eo} e^{-iq})(t_{oe} e^{-iq} + t_{eo} e^{iq})}{t_{eo}^2 (\epsilon_o - E)^2} \\
&= \left[\frac{(t_{oe} e^{iq} + t_{eo} e^{-iq})(t_{oe} e^{-iq} + t_{eo} e^{iq})}{t_{eo}^2 (\epsilon_e - E)(\epsilon_o - E)} \right]^2 \\
&= \left[\frac{t_{eo}^2 + t_{oe}^2 + 2t_{eo} t_{oe} \cos(2q)}{t_{eo}^2 (\epsilon_e - E)(\epsilon_o - E)} \right]^2 \\
&= \left[\frac{(\epsilon_e - E)(\epsilon_o - E)}{t_{eo}^2 (\epsilon_e - E)(\epsilon_o - E)} \right]^2 \\
&= \frac{1}{t_{eo}^4}
\end{aligned} \tag{63}$$

where use has been made of $(\epsilon_e - E)(\epsilon_o - E) = t_{eo}^2 + t_{oe}^2 + 2t_{eo} t_{oe} \cos(2q)$. In addition, one has

$$\begin{aligned}
\Lambda \Lambda^* &= t_{oe}^2 \left(\frac{\delta}{\delta^*} e^{iq} - e^{-iq} \right) \left(\frac{\delta^*}{\delta} e^{-iq} - e^{iq} \right) \\
&= t_{oe}^2 \left(2 - \frac{\delta}{\delta^*} e^{2iq} - \frac{\delta^*}{\delta} e^{-2iq} \right) \\
&= t_{oe}^2 \left[2 \frac{(\epsilon_e - E)(\epsilon_o - E)}{(\epsilon_e - E)(\epsilon_o - E)} - \frac{(t_{eo} e^{iq} + t_{oe} e^{-iq})(t_{oe} e^{-iq} + t_{eo} e^{iq})}{(\epsilon_e - E)(\epsilon_o - E)} e^{2iq} - \frac{(t_{eo} e^{-iq} + t_{oe} e^{iq})(t_{oe} e^{iq} + t_{eo} e^{-iq})}{(\epsilon_e - E)(\epsilon_o - E)} e^{-2iq} \right] \\
&= \frac{t_{oe}^2}{(\epsilon_e - E)(\epsilon_o - E)} \left[2(\epsilon_e - E)(\epsilon_o - E) - (2t_{eo} t_{oe} + t_{eo}^2 e^{2iq} + t_{oe}^2 e^{-2iq}) e^{2iq} - (2t_{eo} t_{oe} + t_{eo}^2 e^{-2iq} + t_{oe}^2 e^{2iq}) e^{-2iq} \right] \\
&= \frac{t_{oe}^2}{(\epsilon_e - E)(\epsilon_o - E)} \left[2(\epsilon_e - E)(\epsilon_o - E) - 2t_{eo} t_{oe} (e^{2iq} + e^{-2iq}) - t_{eo}^2 (e^{4iq} + e^{-4iq}) - 2t_{oe}^2 \right] \\
&= \frac{t_{oe}^2}{(\epsilon_e - E)(\epsilon_o - E)} \left[2t_{eo}^2 - 2t_{eo}^2 \cos(4q) \right] \\
&= \frac{2t_{oe}^2 t_{eo}^2}{(\epsilon_e - E)(\epsilon_o - E)} \left[1 - (2 \cos^2(2q) - 1) \right] \\
&= \frac{2t_{oe}^2 t_{eo}^2}{(\epsilon_e - E)(\epsilon_o - E)} \left[2 - 2 \cos^2(2q) \right] \\
&= \frac{4t_{oe}^2 t_{eo}^2 \sin^2(2q)}{(\epsilon_e - E)(\epsilon_o - E)} \\
&= t_{eo}^4 \gamma_1 \gamma_2^*
\end{aligned} \tag{64}$$

where use has been made of

$$2(\epsilon_e - E)(\epsilon_o - E) - 4t_{eo} t_{oe} \cos(2q) - 2t_{oe}^2 = 2t_{eo}^2 \tag{65}$$

and the double angle formula

$$\cos(4q) = 2 \cos^2(2q) - 1. \tag{66}$$

Consequently we have shown

$$|\xi_w^{-1}|^2 |\xi_u^{-1}|^2 |\Lambda|^2 = \gamma_1 \gamma_2^*. \tag{67}$$

Therefore, in the general case within the TB model, we find the matrix method to obtain $\mathcal{T}(E)$ from Eq. (51) for both dimerized leads and uniform leads to be equivalent to the Green's function method which has

$$\mathcal{T}(E) = \text{Tr}(\mathbf{\Gamma}_1 \mathbf{G} \mathbf{\Gamma}_2 \mathbf{G}^\dagger). \tag{68}$$

APPENDIX F: QUANTUM DRAGON SOLUTION FOR $\ell=2$

The full solution is presented for dimerized leads connected to a simple two-slice ($\ell=2$, $m=1$) device. The

same equations for the transmission are also valid for uniform leads attached to an $\ell=2$ device. For simplicity, we take $\epsilon_o = \epsilon_e = 0$, setting our zero of energy in the problem. This also means for both the incoming and outgoing leads $\xi_w = \xi_u = \xi$. The Green's function method is used, thereby requiring only use of 2×2 matrices. The goal of this section is to show the full solution for the transmission $\mathcal{T}(E)$ for the general case, and show how it simplifies to the quantum dragon solution $\mathcal{T}(E)=1$.

The Hamiltonian for the simple 2 site ($\ell=2$, $m=1$) device is

$$\mathcal{H}_{ab} = \begin{pmatrix} \epsilon_a & -t_{ab} \\ -t_{ab} & \epsilon_b \end{pmatrix} \tag{69}$$

with hopping t_{ab} between the two atoms in the device, and on site energies for the two atoms ϵ_a and ϵ_b . The device is coupled to two dimerized single-channel leads

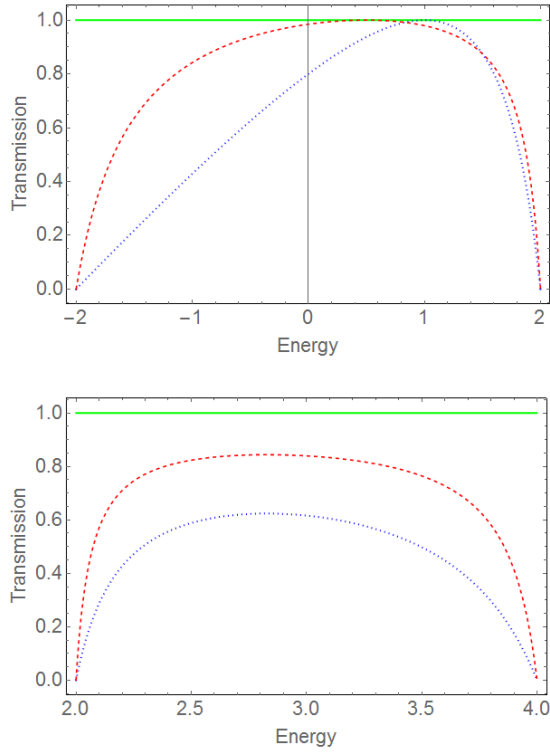


FIG. 8. (Color online.) Transmission \mathcal{T} vs energy E for devices with $m=1$ and $\ell=2$. (Top) Uniform leads. In all three curves $t_{ab}=1$. Shown are the three cases $\epsilon_a=\epsilon_b=1$ (blue, dotted), $\epsilon_a=\epsilon_b=0.5$ (red, dashed), and the quantum dragon solution $\epsilon_a=\epsilon_b=0$ (green, solid). (Bottom) Dimerized leads with $t_{eo}=1$ and $t_{oe}=3$, and all curves have $t_{ab}=t_{oe}=3$. Shown are the same three cases as in the top graph, namely $\epsilon_a=\epsilon_b=1.0$ (blue, dotted), $\epsilon_a=\epsilon_b=0.5$ (red, dashed), and the quantum dragon solution $\epsilon_a=\epsilon_b=0$ (green, solid) of $\mathcal{T}(E) = 1$ for all energies which propagate in the leads. See text in Appendix E for a complete description.

[incoming vector $\vec{w}^\dagger = (-w \ 0)$ and outgoing vector $\vec{u}^\dagger = (0 \ -u)$], giving the self energy matrices

$$\Sigma_1 = \begin{pmatrix} \frac{-w^2}{\xi} & 0 \\ 0 & 0 \end{pmatrix} \quad \text{and} \quad \Sigma_2 = \begin{pmatrix} 0 & 0 \\ 0 & \frac{-u^2}{\xi} \end{pmatrix}. \quad (70)$$

The figure setup is the same as in App. A of ref. 19. It should be noted that the quantity ξ is complex, but both w and u are here taken to be real positive numbers. The complex quantity ξ is different for uniform leads and dimerized leads, namely

$$\xi = \begin{cases} e^{-iq} & \text{uniform} \\ \frac{-E t_{eo} e^{-iq}}{t_{eo} e^{-iq} + t_{oe} e^{iq}} & \text{dimerized} . \end{cases} \quad (71)$$

From Eq.(70), the coupling matrices are expressed as

$$\Gamma_1 = i \left(\Sigma_1 - \Sigma_1^\dagger \right) = iw^2 \begin{pmatrix} \frac{1}{\xi^*} - \frac{1}{\xi} & 0 \\ 0 & 0 \end{pmatrix} \quad (72)$$

and

$$\Gamma_2 = i \left(\Sigma_2 - \Sigma_2^\dagger \right) = iu^2 \begin{pmatrix} 0 & 0 \\ 0 & \frac{1}{\xi^*} - \frac{1}{\xi} \end{pmatrix}. \quad (73)$$

The Green's function, \mathcal{G} is

$$\begin{aligned} \mathcal{G} &= (EI - \mathcal{H} - \Sigma_1 - \Sigma_2)^{-1} \\ &= \begin{pmatrix} \frac{w^2}{\xi} - \kappa_a & t_{ab} \\ t_{ab} & \frac{u^2}{\xi} - \kappa_b \end{pmatrix}^{-1} \end{aligned} \quad (74)$$

with $\kappa_a = \epsilon_a - E$ and $\kappa_b = \epsilon_b - E$. The electron transmission probability can be expressed in terms of the Green's function, \mathcal{G} and the coupling matrices, Γ_1 and Γ_2 as

$$\mathcal{T}(E) = \text{Tr} \left(\Gamma_1 \mathcal{G} \Gamma_2 \mathcal{G}^\dagger \right). \quad (75)$$

Put Eq. (72), Eq. (73) and Eq. (74) into Eq.(75). This gives the electron transmission probability as

$$\mathcal{T}(E) = \frac{w^2 u^2 t_{ab}^2 \Lambda \Lambda^*}{[(w^2 - \kappa_a \xi)(u^2 - \kappa_b \xi) - t_{ab}^2 \xi^2] [(w^2 - \kappa_a \xi^*)(u^2 - \kappa_b \xi^*) - t_{ab}^2 \xi^{*2}]}. \quad (76)$$

In the case when $w = u$, Eq.(76) becomes

$$\mathcal{T}(E) = \frac{w^4 t_{ab}^2 \Lambda \Lambda^*}{[(w^2 - \kappa_a \xi)(w^2 - \kappa_b \xi) - t_{ab}^2 \xi^2] [(w^2 - \kappa_a \xi^*)(w^2 - \kappa_b \xi^*) - t_{ab}^2 \xi^{*2}]}. \quad (77)$$

Eq. (77) is the transmission probability for the two site device coupled to either uniform ($t_{eo}=t_{oe}=t_{lead}$) or dimerized ($t_{eo} \neq t_{oe}$) leads, depending on the value of ξ in Eq. (71) and Λ in Eq. (32).

Furthermore, when $\epsilon_a = \epsilon_b$, Eq. (77) becomes

$$\mathcal{T}(E) = \frac{w^4 t_{ab}^2 \Lambda \Lambda^*}{[(w^2 - \kappa_a \xi)^2 - t_{ab}^2 \xi^2] [(w^2 - \kappa_a \xi^*)^2 - t_{ab}^2 \xi^{*2}]}. \quad (78)$$

A plot of $\mathcal{T}(E)$ for $\ell=2$ for selected parameters is shown in Fig. 8 for both uniform and for dimerized leads.

To see how the quantum dragon solution is obtained from the mathematics, consider a $\ell=2$ and $m = 1$ device with uniform leads ($t_{oe}=t_{eo}=1$), with $w=u=t_{ab}=1$ and $\epsilon_a=\epsilon_b=0$ so $\kappa_a=\kappa_b=-E$. Eq. (78) gives the quantum dragon

solution from the operations

$$\begin{aligned}
\mathcal{T}(E) &= \frac{\Lambda\Lambda^*}{[(1+E\xi)^2-\xi^2][(1+E\xi^*)^2-\xi^{*2}]} \\
&= \frac{4\sin^2(q)}{[(1+Ee^{iq})^2-e^{2iq}][(1+Ee^{-iq})^2-e^{-2iq}]} \\
&= \frac{4-E^2}{[1+2Ee^{iq}+(E^2-1)e^{2iq}][1+2Ee^{-iq}+(E^2-1)e^{-2iq}]} \\
&= \frac{4-E^2}{2+2E^2+E^4+4E\cos(q)+2(E^2-1)\cos(2q)+4E(E^2-1)\cos(q)} \\
&= \frac{4-E^2}{2+2E^2+E^4-2E^2+2(E^2-1)\left(\frac{E^2}{2}-1\right)-2E^2(E^2-1)} \\
&= \frac{4-E^2}{2+2E^2+E^4-2E^2+(E^4-3E^2+2)-2E^4+2E^2} \\
&= \frac{4-E^2}{4-E^2} \\
&= 1.
\end{aligned}$$

This $m = 1$ and $\ell = 2$ device acts as a ‘short circuit’ between the two uniform leads. Because it is a ‘short circuit’, physically the solution $\mathcal{T}(E) = 1$ makes sense. This physical solution should also extend to the case of $m = 1$ and general ℓ , but the algebra becomes more messy than Eq. (79).

Starting from Eq. (78) for the dimerized case, a ‘short

starting, $\kappa_a = \kappa_b = -E$

use $\Lambda = -2i\sin(q)$ and $\xi = e^{iq}$

use $\sin(q) = \frac{\sqrt{4-E^2}}{2}$, expand

multiply out, group terms, use $2\cos(q) = e^{iq} + e^{-iq}$

use $\cos(q) = -\frac{E}{2}$, $\cos(2q) = 2\cos^2(q) - 1$

multiply out

collect terms (many terms cancel)

quantum dragon solution

(79)

circuit’ should be found for even ℓ when $w = u = t_{eo}$, $t_{ab} = t_{oe}$, and $\epsilon_a = \epsilon_b = 0$. However, the algebra becomes very messy in this case, even for a $m = 1$ and $\ell = 2$ device. However, physically one expects a ‘short circuit’ solution in the quantum sense, because the inserted device has the same structure as the leads. This is indeed what we observe numerically, as seen in Fig. 8.

* Also at Faculty of Mathematics and Physics, Charles University, Ke Karlovu 5, CZ-121 16 Praha 2, Czech Republic; man40@msstate.edu

¹ M.M. Waldrop, *The chips are down for Moore’s law*, Nature **530**, 141-147 (2016).

² T. Tsurumi, H. Hirayama, M. Vacha, and T. Taniyama, *Nanoscale physics for materials science* (CRC Press, Boca Raton, FL, 2010).

³ *Nanoelectronics: Materials, Devices, Applications*, two volumes, Edited by R. Puers, L. Baldi, M. van de Voorde, and S.E. van Nooten, (Wiley-VCH, Weinheim, Germany, 2017).

⁴ Datta, S. *Electronic Transport in Mesoscopic Systems* (Cambridge University Press, Cambridge, UK, 1995).

⁵ Ferry, D.K., & Goodnick, S.M. *Transport in Nanostructures* (Cambridge University Press, Cambridge, UK, 1997).

⁶ T.N. Todorov, *Tight-binding simulation of current-carrying nanostructures* J. Phys.: Condens. Matter **14**, 3049-3084 (2002).

⁷ Datta, S. *Quantum Transport: Atom to Transistor* (Cambridge University Press, Cambridge, UK, 2005).

⁸ N.A. Zimbovskaya and M.R. Pederson, *Electron transport through molecular junctions*, Phys. Reports **509**, 1-87 (2011).

⁹ J.C. Cuevas and E. Scheer, *Molecular Electronics: An introduction to theory and experiment*, 2nd edition, (World Scientific, Singapore, 2017).

¹⁰ Landauer, R. *Spatial variation of currents and fields due to localized scatterers in metallic conduction*. IBM J. Research and Development **1**, 223-231 (1957).

¹¹ P.F. Bagwell and T.P. Orlando, *Landauer’s conductance formula and its generalization to finite voltages*. Phys. Rev. B **40**, 1456-1464 (1989).

¹² G.B. Lesovik, *Excess quantum noise in 2D ballistic point contacts*, JETP Lett. **49**, 592-594 (1989).

¹³ M. Büttiker, *Scattering theory of thermal and excess noise in open conductors*, Phys. Rev. Lett. **65**, 2901-2904 (1990).

¹⁴ A. Kumar, L. Saminadayar, D.C. Glatti, Y. Jin, and B. Etienne, *Experimental test of the quantum shot noise reduction theory*, Phys. Rev. Lett. **76**, 2778-2781 (1996).

¹⁵ T. Ouisse, *Electron Transport in Nanostructures and Mesoscopic Devices: An Introduction* (John Wiley & Sons, Hoboken, NJ, 2013).

¹⁶ R. de Picciotto, H.L. Stormer, L.N. Pfeiffer, K.W. Baldwin, and K.W. West, *Four-terminal resistance of a ballistic quantum wire*, Nature **411**, 51-54 (2001).

¹⁷ K. Wakabayashi, Y. Takane, and M. Sigrist, *Perfectly conducting channel and universality crossover in disordered graphene nanoribbons*, Phys. Rev. Lett. **99**, 036601 (2007).

¹⁸ A. Matsumoto, T. Arita, Y. Takane, Y. Yoshimura, and K.-I. Imura, *Manipulating quantum channels in weak topological insulator nanoarchitectures*, Phys. Rev. B **92**, 195424 [14 pages] (2015).

¹⁹ M.A. Novotny, *Energy-independent total quantum transmission of electrons through nanodevices with correlated disorder*, Phys. Rev. B **90**, 165103 [14 pages] (2014).

²⁰ M. Ouyang, J.-L. Huang, C.L. Cheung, and C.M. Lieber, *Energy gaps in “metallic” single-walled carbon nanotubes*, Science **292**, 702-702 (2001).

²¹ J. Kong, E. Yenilmez, T.W. Tombler, W. Kim, and H. Dai, *Quantum interference and ballistic transmission in nanotube electron waveguides*, Phys. Rev. Lett. **87**, 106801 [4 pages] (2001).

²² J. Baringhaus, M. Ruan, F. Edler, A. Tejada, M. Sicot, A. Taleb-Ibrahim, A.-P. Li, Z. Jiang, E.H. Conrad, C. Berger, C. Tegenkamp, and W.A. de Heer, *Exceptional ballistic transport in epitaxial graphene nanoribbons*, Nature **506**, 349-354 (2014).

²³ A. Celis, M.N. Nair, A. Taleb-Ibrahim, E.H. Conrad, C. Berger, W.A. de Heer, and A. Tejada, *Graphene nanorib-*

- bons: fabrication properties and devices, *J. Phys. D: App. Phys.* **49**, 143001 (2016).
- ²⁴ C.T. White and T.N. Todorov, *Carbon nanotubes as long ballistic conductors*, *Nature* **393**, 240-242 (1989).
- ²⁵ D. Erts, H. Olin, L. Ryen, E. Olsson, and A. Thölen, *Maxwell and Sharvin conductance in gold point contacts investigated using TEM-STM* *Phys. Rev. B* **61**, 112725-12727 (2000).
- ²⁶ Daboul, D., Chang, I., & Aharony, A. Series expansion study of quantum percolation on the square lattice. *Euro. J. Phys. B* **16**, 303-316 (2000).
- ²⁷ J. Zhao, Q. Deng, A. Bachmatiuk, G. Sandeep, A. Popov, and J. Eckert, *Free-standing single-atom thick iron membranes suspended in graphene pores*, *Science* **343**, 1228-1232 (2014).
- ²⁸ K. Yin, Y.-Y. Zhang, Y. Zhou, L. Sun, M.F. Chisholm, S.T. Pantelides, and W. Zhou, *Unsupported single-atom-thick copper oxide monolayers*, *2D Mater.* **4**, 011001 [8 pages] (2017).
- ²⁹ E. Kano, D.G. Kvashnin, S. Sakai, L.A. Chernozatonskii, P.B. Sorokin, A. Hashimoto, and M. Takeguchi, *One-atom-thick 2D copper oxide clusters on graphene*, *Nanoscale* **9**, 3980-3985 (2017).
- ³⁰ K.S. Novoselov, A. Mishchenko, A. Carvalho, and A.H. Castro Neto, *2D materials and van der Waals heterostructures*, *Science* **353**, aac9439 [11 pages] (2016).
- ³¹ S. Boettcher, C. Varghese, and M.A. Novotny, *Quantum transport through hierarchical structures*, *Phys. Rev. E* **83**, 041106 [12 pages] (2011).
- ³² M.A. Novotny, L. Solomon, and G. Inkoom, *Quantum transport through a fully connected network with disorder*, *Phys. Procedia* **53**, 71-74 (2014).
- ³³ *Simulation of transport in nanodevices*, Editors F. Triozon and P. Dollfus, (John Wiley & Sons, Hoboken, NJ, 2016).
- ³⁴ A.K. Jain, *A sinusoidal family of unitary transforms*, *IEEE Trans. Pattern Analysis and Machine Intelligence*, **PAMI-1**, 356-365 (1979).
- ³⁵ P.W. Anderson, *Absence of diffusion in certain random lattices*, *Phys. Rev.* **109**, 1492-1505 (1958).
- ³⁶ T. Schwartz, G. Bartal, S. Fishman, and M. Segev, *Transport and Anderson localization in disordered two-dimensional photonic lattices*, *Nature* **446**, 52-55 (2007).
- ³⁷ G. Inkoom, *Quantum dragon solutions for electron transport through single-layer planar rectangular crystals*, Ph.D. Dissertation, Mississippi State University, 2017.
- ³⁸ S. Boettcher, C. Varghese, and M.A. Novotny *Quantum transport through hierarchical structures* *Phys. Rev. B* **83**, 041106 [12 pages] (2011).
- ³⁹ S. Souma and A. Suzuki, *Local density of states and scattering matrix in quasi-one-dimensional systems*, *Phys. Rev. B* **65**, 115307 [7 pages] (2002).
- ⁴⁰ A.E. Miroschnichenko, S. Flach, and Y.S. Kivshar, *Fano resonances in nanoscale structures*, *Rev. Mod. Phys.* **82**, 2257-2298 (2010).
- ⁴¹ V.E. Tarasov, *Exact discretization of Schrödinger equation*, *Physical Letters A* **380**, 68-75 (2016).
- ⁴² C. Flindt, T. Novotný, A. Braggio, M. Sasseti, and A.-P. Jauho, *Counting statistics of non-Markovian quantum stochastic processes*, *Phys Rev. Lett.* **100**, 150601 [4 pages] (2008).
- ⁴³ A. Biborski, A.P. Kadzzielawa, A. Gorzyca-Goraj, E. Zipper, M. Maška, and J. Spalek, *Dot-ring nanostructure: Rigorous analysis of many-electron effects*, *Scientific Reports* **6**, 29887 [14 pages] (2016).
- ⁴⁴ M.A. Novotny, *Materials and devices that provide total transmission of electrons without ballistic propagation and methods for devising same*, U.S. Patent Pending.
- ⁴⁵ Y. Konishi, H. Tokoro, M. Nishino, and S. Miyashita, *Monte Carlo Simulation of Pressure-Induced Phase Transitions in Spin-Crossover Materials* *Phys. Rev. Lett.* **100**, 067206 [4 pages] (2008).
- ⁴⁶ F. Bloch, *Über die Quantenmechanik der Elektronen in Kristallgittern*, *Z. Physik* **52**, 555-600 (1928).